Kramers-Kronig detection in the quantum regime

Thomas Pousset,* Maxime Federico, Romain Alléaume,† and Nicolas Fabre‡
Telecom Paris, Institut Polytechnique de Paris, 19 Place Marguerite Perey, 91120 Palaiseau, France

(Received 26 February 2025; accepted 7 October 2025; published 12 December 2025)

We investigate the quantization of Kramers-Kronig detection technique initially developed for classical optical communications. It consists in mixing the unknown field with a strong monochromatic local oscillator on an unbalanced beam splitter. A single output of the beam splitter undergoes a direct detection of the optical intensity by means of a single photodiode. When the measured output verifies signal processing constraints, namely, the minimal phase and the single-sideband constraints, Kramers-Kronig detection reconstructs the phase of the signal from the intensity measurements via a digitally computed Hilbert transform. The local oscillator being known, Kramers-Kronig detection allows for reconstructing the quadratures of the unknown field. We show that this result holds in the quantum regime up to first order in the local oscillator amplitude and thus that Kramers-Kronig detection acts as a coherent detection able to measure both quadratures, making it a Gaussian measurement similar to double homodyne detection. We also study in detail the phase information measured by Kramers-Kronig detection for bosonic coherent states, monomode pure states, and mixed states. Finally, we propose and investigate a spectral tomography protocol for single-photon states that is inspired by Kramers-Kronig detection and relies on a spectral engineering of the single photon.

DOI: 10.1103/s8jp-l4hf

I. INTRODUCTION

Classical communication links can be decomposed into five parts according to the Shannon model [1]: the encoder, the transmitter, the channel, the receiver, and the decoder. The logical information is encoded into a physical message transmitted through a channel. The receiver compensates for the channel effects to retrieve the transmitted message, which is then decoded. In optical communications, the message is encoded into an electric field that propagates through an underwater optical fiber for subsea communications or through air for free-space communications, for example, and is detected by either a coherent or a direct detector. Direct detection measures only the intensity of the optical field, whereas coherent detection measures both the intensity and phase of the optical field. Thus, for the same bandwidth, direct detection [2,3] captures less information than coherent detection. However, coherent detectors are more expensive and less compact than direct detectors because they require more optical components, such as a local oscillator (LO) and balanced photodiodes, while traditional direct detectors such as intensity modulation-direct detection [2] systems only need a single photodiode. Therefore, direct detection schemes are mostly used for short communication links in environments unsuited for stable operations, while coherent detection schemes are used for long-distance and high-rate communications [3,4].

The most used coherent detections are balanced detections such as the homodyne detection (HD) [5], the double homodyne detection (DHD) also known as the phase diversity detection [6,7], and the heterodyne detection (HRD) [8]. The first reconstructs a single quadrature of the field by coupling the signal to be measured with a local oscillator at the same carrier frequency. The second reconstructs both quadratures by performing two HDs at the cost of an attenuation of the signal. The last one reconstructs both quadratures by downconverting the signal from the optical domain to the radio-frequency domain by coupling it with a local oscillator shifted in frequency more than the bandwidth of the signal, at the cost of a 3 dB signal-to-noise ratio (SNR) reduction.

Recently, a promising alternative to traditional coherent detectors and direct detectors has been proposed under the name of Kramers-Kronig detection (KKD) [9,10]. This detection acts as a coherent detection since both quadratures of the field can be reconstructed, while using only one photodiode. In the classical regime, KKD may be used for high-speed wireless communications [11], for intradatacenter compact wireless-fiber communications [12], for datacenters interconnections [13,14], and outdoor free-space communications [15]. KKD consists first in mixing a LO with a spectrally engineered signal on a beam splitter such that the LO and the signal are separated in frequency by less than the signal bandwidth. KKD reconstructs the phase of the signal by digitally processing the measured field intensity, which allows recovering both quadratures. KKD highly relies on digital signal processing instead of optical engineering and shifts the optical

*Contact author: thomas.pousset@telecom-paris.fr
†Contact author: romain.alleaume@telecom-paris.fr
‡Contact author: nicolas.fabre@telecom-paris.fr

Published by the American Physical Society under the terms of the Creative Commons Attribution 4.0 International license. Further distribution of this work must maintain attribution to the author(s) and the published article's title, journal citation, and DOI.

complexity into a signal processing complexity to retrieve the phase of the signal [3,16,17].

In practice, when measuring the quadratures, several noises have to be taken into account, such as the quantum fluctuations, the thermal noise, and the phase noise, for example. In the quantum regime, namely, when the SNR is low, the main noise is due to quantum fluctuations and thus the electromagnetic field and the detection must be described by using the quantum optics formalism. Coherent detections [4,18] such as HD [19–22], HHD [23], and HRD [21,24] have been thoroughly analyzed in this regime. They are used in many quantum technology protocols such as quantum random number generators [25,26], quantum tomography [27–29], quantum sensing [30–32], or continuous variable quantum key distribution [33–40].

For KKD, quantum fluctuations have been calculated in Ref. [41], assuming that it measures both quadratures of the field. The SNRs associated with quantum fluctuations on the measurement of a symbol encoded in a coherent state using KKD are reported to be smaller compared to those of HRD, and by extension, DHD, as these two have the same SNR [4]. In Ref. [41], the symbols are carried by plane waves instead of normalized spectral modes. In addition, only a finite number of plane waves are taken into account in the decomposition of the bosonic operators. The consequence is that the symbol can be reconstructed by multiplying the reconstructed signal with the complex conjugated plane wave instead of projecting on a mode with an integral as it is done in classical communications [42]. This leads to time-dependent nonisotropic symbol fluctuations where in one direction the fluctuations drop to $1/6$ while still being $1/2$ on the orthogonal direction, which departs from the DHD model in which quantum fluctuations are isotropic and equal to $1/2$. This result is contradictory to Heisenberg inequality since the product of the two gives a value smaller than $1/4$. It is also claimed in Ref. [43] that the fluctuations when measuring a symbol with KKD are smaller than in DHD because there is no halving of the signal with a balanced beam splitter and thus the SNR is the same as that of HD. However, it has been shown that the 3 dB loss in DHD is fundamentally necessary from a quantum optics perspective—this loss ensures compliance with the Heisenberg algebra when simultaneously measuring conjugate quadratures [4]. While there is no 3 dB loss in SNR from another input of a beam splitter as in DHD, there is a 3 dB loss coming from an orthogonal spectral mode in KKD as we will discuss.

In this article, we show differently that KKD is operationally similar to DHD as it can measure both quadratures of the field with a 3 dB SNR loss compared to HD. After postprocessing, and at the first order of the power of the LO, KKD lies in the class of Gaussian measurements. We consider a model where optical and signal processing are ideal and where the electronics is noiseless and linear, so that the only noise source stems from quantum fluctuations. Unlike in Ref. [41], we consider normalized spectral modes instead of plane waves using the formalism of Refs. [44–46] as the carrier of the symbols. In this context, the natural way to retrieve a symbol from a signal is to filter the signal with the associated spectral mode [42]. By contrast with Ref. [43], we show that, even though there is no halving of the signal such as in DHD, the SNR is still halved for coherent states because of a coupling with an orthogonal spectral mode. We stress that the proof of having the same SNR for the KKD in the quantum regime as for DHD strongly relies on the spectral degree of freedom of light, also crucial in the classical analysis of KKD. This is particularly important due to the Single-side-band constraint (SSB) constraint [9,10] that plays a crucial and different role in the quantum regime of KKD.

In addition, we employ a formulation of KKD that uses a well-defined Hermitian phase operator at time t that is related to the intensity operator at all time by a Hilbert transform. We stress that the phase operator that is defined in this manuscript—and its related first and second moments—obtained through KKD is not the phase operator obtained by a polar decomposition of the annihilation operator defined in the quantum optics literature [47–53]. Indeed, in these references, the introduced exponential of the phase operator does not commute with the number or intensity operator. Instead, the KKD phase operator is a different phase operator whose average value with respect to quasiclassical state matches the phase of a classical optical field. In order to clarify the sense of the KKD phase operator, we investigate the phase that the detection reconstructs for some particular states like, e.g., bosonic coherent states (defined in Refs. [45,54]), mixed states, and monomode pure states. We emphasize that KKD allows in any case obtaining the relative phase between the known local oscillator and the quantum state of interest. As we shall see, the phase of the measured quantum state contains the information about both its particle-number statistics and its temporal mode structure.

Finally, we propose and analyze a KKD-based spectral tomography scheme for reconstructing the phase of the temporal wavefunction of single-photon states [44,55] using time-of-arrival-resolved detection [56]. This approach enables full spectral tomography of single-photon states, as demonstrated in previous experimental works [57–61]. Specifically, the protocol aims to reproduce the temporally resolved intensity typically measured with a PIN photodiode—subject to the aforementioned mathematical constraints—through the measurement of the temporally resolved single-photon probability distribution such that the phase in the two cases can be reconstructed using the Kramers-Kronig (KK) relation. In our proposed protocol, the single-photon state is spectrally engineered such that it corresponds to the coherent superposition of a large monochromatic part and a temporal structure of interest that verifies the minimal phase (MP) [62] and the single-sideband [9,10] conditions. We also suggest a possible experimental implementation of the spectral engineering that relies on electro-optic modulators (EOMs) [63–66], optical spectral filters, and a temporally resolved single-photon detector. The measurement of the time-of-arrival probability single-photon distribution is then used for reconstructing the phase of the single-photon state wavefunction from phase-intensity KKD relations.

The article is organized as follows. In Sec. II, we introduce HD and DHD as examples of coherent detections. We derive their measured operators and the associated quantum fluctuations, as well as the SNR for coherent states. In Sec. III, we study KKD both in the classical regime and in the quantum regime where we derive its measured operators. In Sec. IV, we investigate the phase information reconstructed by KKD

for specific states such as bosonic coherent states, mixed quantum states, and pure monomode states. In Sec. V, we present a single-photon spectral tomography scheme inspired from KKD. Finally, in Sec. VI, we summarize our results and open perspectives.

II. COHERENT DETECTIONS: HOMODYNE DETECTION AND DOUBLE HOMODYNE DETECTION

In typical coherent communications, the emitter sends complex symbols each associated with a spectral narrowband mode of light localized spectrally around a carrier frequency ω_c (for instance, using telecom wavelength, i.e., 1550 nm) in a spatial mode of an optical fiber. In this context, coherent detection [4] is a class of measurements able to measure the quadratures of the field. The most used coherent detection schemes are HD and DHD that often serve as theoretical baselines for characterizing coherent detections.

In this section, we present the quantization of the HD and DHD using a similar formalism as in Refs. [46,67,68], which allows us to introduce the future notation for the KKD in the next section. We will consider ideal optics, noiseless and linear electronics, meaning that the only noise taken into account is the quantum noise. HD allows measuring a single quadrature of light in a mode specified by the LO, the electronics, and the signal processing. DHD allows measuring both quadratures of light in a mode specified by the LO, the electronics, and the signal processing, at the cost of an extra 3 dB loss in SNR on each quadrature compared to HD for coherent states.

A. Homodyne detection

HD starts by mixing the bosonic field in input mode a of interest with a LO in input mode b. The annihilation bosonic operators in mode a, b at time t are denoted by $\hat{a}(t), \hat{b}(t)$. In Appendix A, we remind a detailed introduction of the quantization of the electromagnetic field, where the notations are more detailed. The two input modes are combined into a balanced beam splitter as shown in Fig. 1(a). The outputs of the beam splitter $\hat{c}(t) = (\hat{a}(t) + \hat{b}(t))/\sqrt{2}$ and $\hat{d}(t) = (\hat{a}(t) - \hat{b}(t))/\sqrt{2}$ undergo identical optical path and are measured by identical photodiodes with response function $h(t)$ and unit efficiency. Nonunit efficiency photodiodes can be taken into account as in Ref. [22] by formally putting a beam splitter just before the photodiodes. We assume the LO to be classical and replace the bosonic operator $\hat{b}(t)$ by the classical number (c-number) $Af(t)$, where $A = |A|e^{i\theta}$ is the amplitude and $f(t)$ is the normalized temporal mode of the LO, meaning that $\int \mathrm{d}t|f(t)|^2 = 1$. The difference of the photocurrents [67,68] is written as

$$\begin{aligned}\hat{I}_-(t) &= \int_{-\infty}^{\infty} \mathrm{d}\tau h(t-\tau)(\hat{c}^\dagger(\tau)\hat{c}(\tau) - \hat{d}^\dagger(\tau)\hat{d}(\tau)) \\ &= \int_{-\infty}^{\infty} \mathrm{d}\tau h(t-\tau)(A^* f^*(\tau)\hat{a}(\tau) + Af(\tau)\hat{a}^\dagger(\tau)). \quad (1)\end{aligned}$$

In practice, the integration is performed over a finite time window chosen to fully contain the temporally bounded signal of interest. For a large enough time window, the integration window can be extended to $(-\infty, \infty)$ formally as done above.

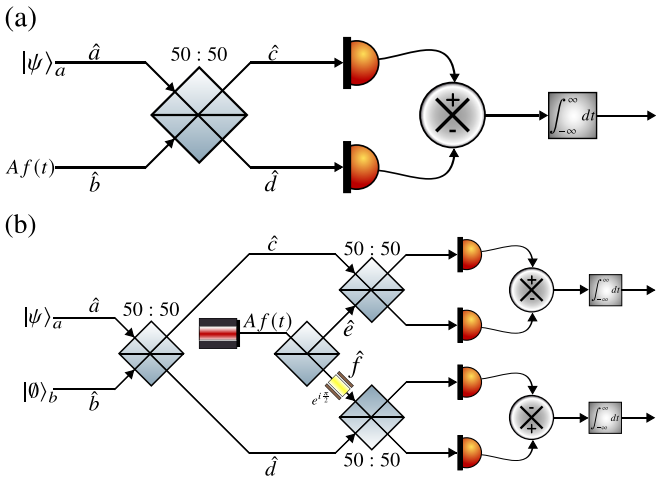


FIG. 1. Setups for (a) homodyne detection and (b) double homodyne detection. Homodyne detection [panel (a)] allows for measuring a single quadrature of light. It consists in mixing the signal of interest in the port $\hat{a}$ with a strong local oscillator in the port $\hat{b}$ on a balanced beam splitter. The intensities of both outputs $\hat{c}$ and $\hat{d}$ are measured with identical photodiodes. The difference of the photocurrents is integrated and is shown to be proportional to the quadrature of the signal to measure at the phase defined by the local oscillator and in the spectral mode defined by the local oscillator. For the output to match the quadratures in expectation value, it has to be renormalized by measuring vacuum fluctuations. Double homodyne detection [panel (b)] allows for measuring both quadratures of light at the cost of an extra vacuum noise. The signal of interest is split in two on a balanced beam splitter. Each part is measured by two identical homodyne detections with the only difference being the phase of the local oscillator. The first homodyne detection phase is zero to measure the position quadrature and the second one is $\pi/2$ to measure the momentum quadrature. As a result from the initial splitting, an extra vacuum noise corresponding to the second input of the first beam splitter is added to the measurement results.

The output of HD is obtained by integrating $\hat{I}_-(t)$ and is proportional to the quadrature of the field of interest:

$$\hat{o}_{\mathrm{HD}} = \int_{-\infty}^{\infty} \mathrm{d}t\hat{I}_-(t) = \hat{x}_\theta^a[\tilde{\xi}]\sqrt{\int \mathrm{d}\tau|\xi(\tau)|^2}, \quad (2)$$

where $\hat{x}_\theta^a[\tilde{\xi}] = (e^{-i\theta}\hat{a}[\tilde{\xi}] + e^{i\theta}\hat{a}^\dagger[\tilde{\xi}])/2$ denotes the quadrature of the input $\hat{a}(t)$ of phase θ in the temporal mode $\tilde{\xi}$ (see Appendix A). The function $\xi(\tau) = 2|A|f(\tau)\int \mathrm{d}t h(t-\tau)$ is defined by the modulus of the amplitude of the LO, the spectral mode of the LO, and the characteristics of the photodiodes. Hence, $\tilde{\xi}(t) = \xi(t)/\sqrt{\int \mathrm{d}\tau|\xi(\tau)|^2}$ is the temporal mode of the measurement that also depends on the LO, the photodiodes, and the electronics in general.

For the output to match the quadrature of the signal of interest, the output is divided by $\sqrt{\int \mathrm{d}\tau|\xi(\tau)|^2}$ to be normalized. To measure the normalization factor, the variance with the input of interest in the vacuum state $|0\rangle_a$ is measured:

$$\Delta^2_{|0\rangle_a}\hat{o}_{\mathrm{HD}} = \frac{1}{4}\int \mathrm{d}\tau|\xi(\tau)|^2, \quad (3)$$

and it allows to renormalize for all next measurements as

$$\hat{o}_{\mathrm{HD}} \longleftarrow \frac{\hat{o}_{\mathrm{HD}}}{2\sqrt{\Delta^2_{|0\rangle_a}\hat{o}_{\mathrm{HD}}}} = \hat{x}^a_\theta[\tilde{\xi}], \tag{4}$$

which is the quadrature of the field of interest. Additionally, due to HD being balanced, technical noises present on both detectors are canceled, provided the photodiodes are identical and the common mode rejection ratio is large [69].

Injecting now a coherent state defined by $|\alpha\rangle = \exp(\alpha\hat{a}^\dagger[\chi] - \alpha^*\hat{a}[\chi])\,|0\rangle$, with $\alpha \in \mathbb{C}$, yields

$$\begin{aligned} \langle\alpha|\,\hat{o}_{\mathrm{HD}}\,|\alpha\rangle &= \mathrm{Re}\{e^{i\theta}\alpha\langle\tilde{\xi},\chi\rangle\},\\ \Delta^2_{|\alpha\rangle}\hat{o}_{\mathrm{HD}} &= \tfrac{1}{4}, \end{aligned} \tag{5}$$

where we have defined the scalar product $\langle\tilde{\xi},\chi\rangle = \int \mathrm{d}t\tilde{\xi}^*(t)\chi(t)$, which is the overlap between the mode of the coherent state χ and the mode of the overall detection $\tilde{\xi}$. Therefore, the expectation value of $\hat{o}_{\mathrm{HD}}$ is the quadrature of angle θ of the coherent states if the spectral mode of the state matches the spectral mode of the HD. Then, the SNR becomes

$$\mathrm{SNR}_{\mathrm{HD}} = \frac{\langle\alpha|\,\hat{o}_{\mathrm{HD}}\,|\alpha\rangle}{\Delta^2_{|\alpha\rangle}\hat{o}_{\mathrm{HD}}} = 4\mathrm{Re}\{e^{-i\theta}\alpha\}. \tag{6}$$

B. Double homodyne detection

While HD measures a single quadrature of light, DHD allows measuring the two orthogonal quadratures of light with a setup as shown in Fig. 1(b). It consists of splitting the signal of interest in two with a first balanced beam splitter, where the output annihilation operators at time t are given by $\hat{c}(t) = \frac{1}{\sqrt{2}}(\hat{a}(t) + \hat{b}(t))$ and $\hat{d}(t) = \frac{1}{\sqrt{2}}(\hat{a}(t) - \hat{b}(t))$. Now, $\hat{b}(t)$ denotes the second input of the first beam splitter of the splitted signal of interest. The outputs c and d are then detected with two HDs, one with an angle $\theta = 0$ to measure the position quadrature $\hat{q}$ and one with an angle $\theta = \pi/2$ to measure the momentum quadrature $\hat{p}$. The LOs used for the two HDs, in spatial modes e and f, are taken in the classical limit and are replaced by c-numbers, $|A|f(t)/\sqrt{2}$ and $|A|e^{i\pi/2}f(t)/\sqrt{2}$. The $\sqrt{2}$ factor comes from the fact that the same laser is split into two to generate both LOs. Using the results of Sec. II A, the two unnormalized outputs are written as

$$\begin{aligned} \hat{o}^{(q)}_{\mathrm{DHD}} &= (\hat{q}_a[\tilde{\xi}] + \hat{q}_b[\tilde{\xi}])\sqrt{\int \mathrm{d}\tau|\xi(\tau)|^2},\\ \hat{o}^{(p)}_{\mathrm{DHD}} &= (\hat{p}_a[\tilde{\xi}] - \hat{p}_b[\tilde{\xi}])\sqrt{\int \mathrm{d}\tau|\xi(\tau)|^2}, \end{aligned} \tag{7}$$

where $\xi(\tau) = |A|f(\tau)\int \mathrm{d}t h(t-\tau)$ is defined similarly as in HD by the amplitude of the LO, the spectral mode of the LO, and the characteristics of the photodiodes, and $\tilde{\xi}(t)$ is the normalized mode associated with $\xi(t)$. Again, as in HD, the outputs must be renormalized *a posteriori* so that they match the quadratures of the signal of interest in expectation value. When the input $\hat{a}(t)$ is kept empty, the variances on the measured operators are

$$\begin{aligned} \Delta^2_{|0\rangle_{ab}}\hat{o}^q_{\mathrm{DHD}} &= \frac{1}{2}\int \mathrm{d}\tau|\xi(\tau)|^2,\\ \Delta^2_{|0\rangle_{ab}}\hat{o}^p_{\mathrm{DHD}} &= \frac{1}{2}\int \mathrm{d}\tau|\xi(\tau)|^2, \end{aligned} \tag{8}$$

which allows us to renormalize the outputs as follows:

$$\begin{aligned} \hat{o}^q_{\mathrm{DHD}} &\longleftarrow \frac{\hat{o}^q_{\mathrm{DHD}}}{\sqrt{2}\sqrt{\Delta^2_{|0\rangle_{ab}}\hat{o}^q_{\mathrm{DHD}}}} = \hat{q}_a[\tilde{\xi}] + \hat{q}_b[\tilde{\xi}],\\ \hat{o}^p_{\mathrm{DHD}} &\longleftarrow \frac{\hat{o}^p_{\mathrm{DHD}}}{\sqrt{2}\sqrt{\Delta^2_{|0\rangle_{ab}}\hat{o}^p_{\mathrm{DHD}}}} = \hat{p}_a[\tilde{\xi}] - \hat{p}_b[\tilde{\xi}]. \end{aligned} \tag{9}$$

In this form, the outputs consist of the quadratures to be measured and additional terms corresponding to the quadratures of the second input of the first beam splitter, referred to as vacuum noise.

If the input state is now a coherent state $|\alpha\rangle$ in the same spectral mode as the one of the detectors, the moments of the outputs of DHD are

$$\begin{aligned} \langle\alpha|\,\hat{o}^q_{\mathrm{DHD}}\,|\alpha\rangle &= \mathrm{Re}\{\alpha\}, \quad \langle\alpha|\,\hat{o}^p_{\mathrm{DHD}}\,|\alpha\rangle = \mathrm{Im}\{\alpha\},\\ \Delta^2_{|\alpha\rangle}\hat{o}^q_{\mathrm{DHD}} &= \tfrac{1}{2}, \quad \Delta^2_{|\alpha\rangle}\hat{o}^p_{\mathrm{DHD}} = \tfrac{1}{2}, \end{aligned} \tag{10}$$

and the SNR for a single quadrature is then

$$\mathrm{SNR}^q_{\mathrm{DHD}} = 2\mathrm{Re}\{\alpha\}, \quad \mathrm{SNR}^p_{\mathrm{DHD}} = 2\mathrm{Im}\{\alpha\}, \tag{11}$$

which is half that of HD. This result is the famous DHD 3 dB loss for the SNR compared to HD.

III. KRAMERS-KRONIG DETECTION

KKD is a direct detection that relies on signal engineering to recover the phase of the measured signal [9,10]. A setup for KKD is presented in Fig. 2(a). It consists of mixing a signal of interest and a monochromatic reference in the form of a LO on an unbalanced beam splitter and measuring a single output. It has been shown that under MP constraint and SSB constraint, it is possible to reconstruct the phase of $\hat{c}(t)$ from its intensity through a Hilbert transform.

In this section, we present the results in the classical regime and the necessary constraints for KKD to work. Then, we present our results in the quantum regime and show that KKD allows reconstructing both quantum quadratures of the field at the cost of an extra vacuum noise coming from an independent spectral mode.

A. Kramers-Kronig detection in the classical regime

In the classical regime, for performing the phase reconstruction using the KK relation, the MP constraints must be verified. The LO is monochromatic with no phase at the carrier frequency, which means that its amplitude can be written as $b(t) = A$. The amplitude A is assumed to be real and thus defines a phase reference. In order to satisfy the MP constraint, the LO contribution must be greater than the signal to be measured [62]:

$$\tilde{r}A > \tilde{t}|a(t)|. \tag{12}$$

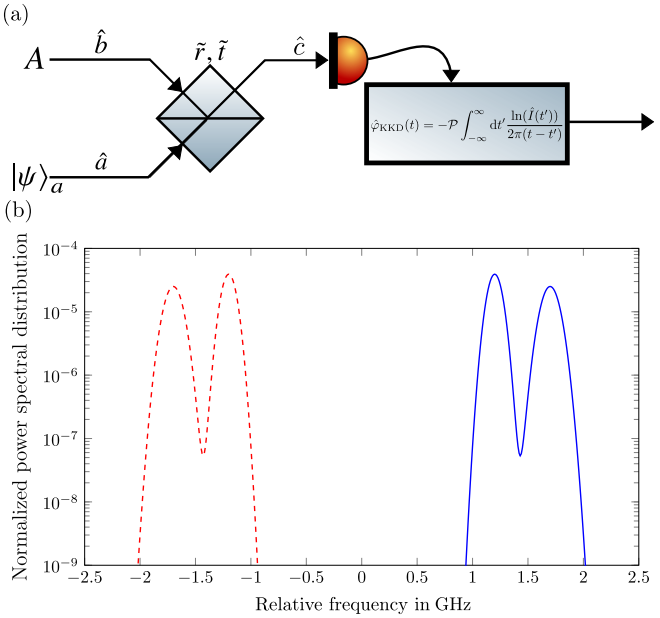


FIG. 2. (a) Setup for Kramers-Kronig detection and (b) example of single-sideband signal. For Kramers-Kronig detection [panel (a)], the signal of interest is injected in the $\hat{a}$ input of a *highly unbalanced* beam splitter while a monochromatic strong and classical local oscillator is injected in the $\hat{b}$ input. The signal of interest verifies the single-sideband constraint. A single output $\hat{c}$ intensity is measured by a photodiode and the intensity at each instant is recorded. The phase of the output $\hat{c}$ is reconstructed by taking the Hilbert transform of the logarithm of the measured intensity. Since the local oscillator is known, it is possible to reconstruct the input of interest $\hat{a}$ with the reconstructed $\hat{c}$ output. Single-sideband signals [panel (b)] are signals spectrally on the right of the carrier frequency represented here by the zero value. The plain (blue) signal is an example of the spectrum of a single-sideband mode (logarithmic scale), whereas the dashed (red) signal is the complex conjugate of the blue signal and is not a single-sideband mode as it lies on the left of the carrier frequency. For Kramers-Kronig, this conjugated spectral mode is a source of extra noise.

Additionally, the input of interest must verify the SSB constraint that consists in $a(t)$ being spectrally on the right of the LO, i.e.,

$$\mathcal{F}(a)(\omega \leqslant 0) = 0, \tag{13}$$

where $\mathcal{F}(f)(\omega) = \int_{-\infty}^{\infty} \mathrm{d}t\, f(t) e^{i\omega t}$ denotes the Fourier transform with ω the relative frequency with respect to the carrier frequency. When the MP constraint is verified, the logarithm of the output $c(t) = \tilde{r}A + \tilde{t}a(t)$, where $\tilde{r}$ and $\tilde{t}$ are, respectively, the reflection and transmission coefficients of the beam splitter, can be expressed as a power series since $\tilde{r}A > \tilde{t}|a(t)|$:

$$\begin{aligned}\ln(c(t)) &= \ln(\tilde{r}A + \tilde{t}a(t)) \\ &= \ln(\tilde{r}A) + \sum_{n=0}^{\infty} (-1)^n \frac{\tilde{t}^n a(t)^n}{\tilde{r}^n A^n n}.\end{aligned} \tag{14}$$

The total term is also SSB since convolutions in frequency of SSB functions are SSB functions. On the other hand, the logarithm of the $c(t)$ output can be expressed in terms of the phase $\arg(c(t))$ and the intensity $I(t) = |c(t)|^2$ as follows:

$$\ln(c(t)) = \tfrac{1}{2}\ln(I(t)) + i\arg(c(t)). \tag{15}$$

Since the total expression is SSB, it verifies traditional Kramers-Kronig relations for electrical susceptibilities [70] where the time and frequency have been swapped. The intensity being measurable, it is possible to reconstruct the phase from the time measurement results [9,10] with a Hilbert transform [71], i.e.,

$$\varphi_{\mathrm{KKD}}(t) = -\mathcal{P}\int_{-\infty}^{\infty} \mathrm{d}t' \frac{\ln(I(t'))}{2\pi(t-t')}, \tag{16}$$

where $\varphi_{\mathrm{KKD}} = \arg(c(t))$ in the classical regime and where $\mathcal{P}$ denotes Cauchy principal value [71]. The output $c(t)$ is reconstructed as follows: $c(t) = \sqrt{I(t)}e^{i\varphi_{\mathrm{KKD}}(t)}$ and the input signal reads

$$a(t) = \frac{c(t) - \tilde{r}A}{\tilde{t}} = \frac{\sqrt{I(t)}e^{i\varphi_{\mathrm{KKD}}(t)} - \tilde{r}A}{\tilde{t}}. \tag{17}$$

The complex symbols and the quadratures for a given spectral mode $f(t)$ are finally recovered with a projection integral:

$$\begin{aligned} a[f] &= \int_{-\infty}^{\infty} \mathrm{d}t\, f^*(t)a(t), \\ q[f] &= \frac{a[f] + a^*[f]}{2}, \\ p[f] &= \frac{a[f] - a^*[f]}{2i}, \end{aligned} \tag{18}$$

where $f(t)$ is an SSB mode. Indeed, $a(t)$ is supposed to be only composed of SSB modes to verify the SSB constraint. Since both quadratures can be recovered, KKD is indeed a direct detection acting as a coherent detection measuring both quadratures in the classical regime.

B. Kramers-Kronig detection in the quantum regime

The quantization of the inputs $a(t)$ and $b(t)$ and the output $c(t)$ leads to their replacement as bosonic quantum operators $\hat{a}(t)$, $\hat{b}(t)$, and $\hat{c}(t)$, similarly to what was done in Sec. II A.

Comparatively to traditional balanced detections, only a single output of the beam splitter is measured for KKD and thus the second output is formally traced out. In the case of coherent states at both inputs, this tracing operation does not modify the state of the measured output since the output state is a product of two coherent states. However, for a general state at the input, the tracing out operation will introduce a supplementary noise. To circumvent this, we propose to use a highly unbalanced beam splitter to mitigate the effect of the trace on the second output. The beam splitter must satisfy the condition $\tilde{t} \to 1$, ensuring that the fluctuations in the nonmeasured output do not impact the signal of interest. The reflection coefficient must then be $\tilde{r} \to 0$ and thus the local oscillator amplitude must be chosen accordingly.

We treat the case of a classical LO, meaning that $\hat{b}(t)$ is replaced by a c-number A, since the LO is still monochromatic. We decompose it as a modulus and a phase: $A = A_0 e^{i\theta}$. For practical purposes, we extend the MP constraints to an asymptotic form, which allows us to perform a Taylor expansion of the logarithm in the reconstructed phase, defined in Eq. (16):

$$\tilde{r}A_0 \gg \tilde{t}|\langle a(t)\rangle|, \tag{19}$$

where the expectation value is taken on the unknown state of interest. This asymptotic constraint is verified in practice for traditional coherent detections in quantum optics protocols since the LO is supposed to be classical and the quantum signal to measure is supposed to be of only few photons. The intensity of a single output, $\hat{I}(t) = \hat{c}^\dagger(t)\hat{c}(t)$, is measured:

$$\hat{I}(t) = \tilde{r}^2 A_0^2 + \tilde{r} A_0(\hat{a}(t)e^{-i\theta} + \hat{a}^\dagger(t)e^{i\theta}) + \hat{a}^\dagger(t)\hat{a}(t), \quad (20)$$

where each term is in baseband domain unlike in HRD where the LO-signal term of interest is in radio-frequency domain.

Performing the Hilbert transform on the logarithm of the intensity defines a KKD phase operator written as

$$\hat{\varphi}_{\mathrm{KKD}}(t) = -\mathcal{P}\int_{-\infty}^{\infty} \mathrm{d}t' \frac{\ln(\hat{I}(t'))}{2\pi(t-t')}. \quad (21)$$

This phase operator is well defined for the states under consideration, Hermitian, and commutes with the intensity, making it fundamentally different from the phase operator of the quantum optics literature that is not Hermitian and does not commute with the number operator [47–51,53] (see Appendix C for a detailed description). Indeed, since A is asymptotically large, the state of the field at output $\hat{c}$ has infinitesimally small overlap with the vacuum state and thus the issue of the intensity operator not being invertible is avoided, which allows the application of the logarithm operation [72]. Taking into account the strong classical monochromatic LO, and thus that $\hat{I}(t) \approx \tilde{r}^2 A^2 + \tilde{r} A(\hat{a}^\dagger(t)e^{i\theta} + \hat{a}(t)e^{-i\theta})$ at first order, the logarithm is Taylor expanded. The phase $\hat{\varphi}_{\mathrm{KKD}}(t)$ is then written as a function of the quadrature operators associated with all plane waves of positive frequency relative to the carrier:

$$\hat{\varphi}_{\mathrm{KKD}}(t) = \int_0^\infty \frac{\mathrm{d}\omega}{2\pi}\frac{\tilde{t}}{\tilde{r}}\frac{1}{A}[(\hat{p}_\theta(\omega) - \hat{p}_\theta(-\omega))\cos(\omega t) - (\hat{q}_\theta(\omega) + \hat{q}_\theta(-\omega))\sin(\omega t)] + O\left(\frac{1}{A_0^2}\right), \quad (22)$$

where $O(1/A_0^2)$ denotes an operator of expectation and cumulants of order $O(1/A_0^2)$ and where $\hat{q}_\theta(\omega)$ and $\hat{p}_\theta(\omega)$ denote the quadratures at frequency ω rotated by θ or in other words the quadratures of $\hat{a}(\omega)e^{-i\theta}$ (see Appendix B for a detailed derivation of this result). The KKD phase operator allows reconstructing the imaginary part of the field given the real part contained in the LO-signal term measured in the intensity. In contrast, for HRD, for example, the intensity signal belonging in the radio-frequency domain undergoes in-phase and quadrature (IQ) demodulation instead of KKD signal processing.

We define the polar decomposition of the annihilation operator at time t from the intensity and phase operators that are measured as $\hat{c}_{\mathrm{KKD}}(t) = \sqrt{\hat{I}(t)}e^{i\hat{\varphi}_{\mathrm{KKD}}(t)}$, inspired by the polar decomposition of the phase operator in a given mode [47,48,52]. The reconstructed input of interest, at first order of the LO intensity, can thus be written as

$$\hat{a}_{\mathrm{KKD}}(t) = \frac{\hat{c}_{\mathrm{KKD}}(t) - \tilde{r}A}{\tilde{t}} = \int_0^\infty \frac{\mathrm{d}\omega}{2\pi}(\hat{a}(\omega)e^{-i\theta} + \hat{a}^\dagger(-\omega)e^{i\theta})e^{i\omega t} + O\left(\frac{1}{A_0}\right). \quad (23)$$

The signal components at negative relative frequency appear in the reconstructed signal, even though the emitted signal is supposed to be SSB. This contribution corresponds to vacuum contribution and will have an impact on the calculation of fluctuations. The quadratures in a given SSB spectral mode $f(t)$ can be reconstructed with a projection integral yielding the final result

$$\hat{o}^q_{\mathrm{KKD}}[f] = \hat{q}_\theta[f] + \hat{q}_\theta[f^*] + O\left(\frac{1}{A_0}\right), \quad \hat{o}^p_{\mathrm{KKD}}[f] = \hat{p}_\theta[f] - \hat{p}_\theta[f^*] + O\left(\frac{1}{A_0}\right), \quad (24)$$

where again, $\hat{q}_\theta[f]$ and $\hat{p}_\theta[f]$ correspond to the quadratures rotated by θ or in other words the quadratures of $\hat{a}[f]e^{-i\theta}$, and the extra quadrature operators associated with the mode $f^*(t)$ correspond to vacuum fluctuations. Indeed, in our convention, the mode $f^*(t)$ corresponds to a spectral mode of negative frequency relative to the carrier frequency. An example is shown in Fig. 2(b), where the plain (blue) spectrum corresponds to an SSB mode $f(t)$ and the dashed (red) spectrum corresponds to the complex conjugate $f^*(t)$. This shows that KKD is equivalent to DHD since both measure the two orthogonal quadratures of light with an extra vacuum noise penalty. However, unlike DHD, the extra vacuum noise comes from an empty independent spectral mode for KKD instead of an independent input mode of a beam splitter. Additionally, the quadratures measured may be rotated by controlling the phase of the local oscillator.

C. Discussion regarding experimental implementation

In the case of a practical implementation, several things have to be taken into account. First, in order to perform the subtraction of Eq. (23) it is necessary to know the local oscillator amplitude A beforehand. The phase of A serves as a phase reference since it is assumed to be real. The modulus of A must be measured before performing the KKD coherent detection scheme. Secondly, in Sec. III B the quantities are written in normalized unit such that the variances of the quadratures for vacuum give $1/2$. The measurements must then be renormalized for the outputs to match the quadratures in expectation value. The process is the same as that for DHD: The variance for vacuum is measured and the next measurements are renormalized by the vacuum variance that gives

$$\hat{o}^q_{\mathrm{KKD}} \longleftarrow \frac{\hat{o}^q_{\mathrm{KKD}}}{\sqrt{2}\sqrt{\Delta^q_{|0\rangle_a}\hat{o}^q_{\mathrm{KKD}}}}, \quad \hat{o}^p_{\mathrm{KKD}} \longleftarrow \frac{\hat{o}^p_{\mathrm{KKD}}}{\sqrt{2}\sqrt{\Delta^p_{|0\rangle_a}\hat{o}^p_{\mathrm{KKD}}}}. \quad (25)$$

In Fig. 3, we show a simulation of a symbol reconstruction with KKD. In this simulation, the simulated state to be measured is a classical mixture of random coherent states belonging to a four quadrature amplitude modulation (QAM) [42] constellation with an average of ten photons per symbols. The temporal mode for each symbol is a time-shifted Gaussian. The local oscillator is a known classical monochromatic signal and has an intensity of 10^5 photons s^{-1}. The source for quantum noise is generated at the photodiode. The output current follows a Gaussian law of variance corresponding to

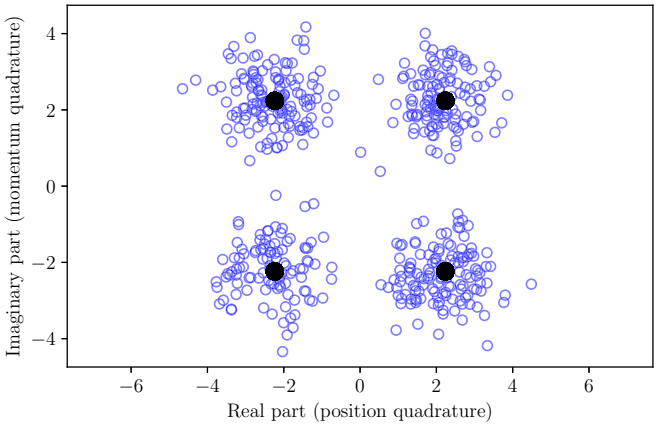


FIG. 3. Simulation of a symbol reconstruction process with Kramers-Kronig detection (phasor diagram). The empty circle markers (blue) denote the measured symbols, whereas the full circles (black) denote the emitted symbols. The emitted symbols are coherent states belonging to a four-QAM constellation and are each associated with a time-shifted Gaussian pulse of bandwidth 22 GHz. Each pulse is composed of ten photons in average. The simulated link is a back-to-back link where the emitter directly sends into the receiver. Finally, the quantum noise is generated at the photodiode where the output photocurrent follows a Normal law with variance that of $\hat{I}(t)$ when the local oscillator is taken classical and completely deterministic.

the variance of $\hat{I}(t)$ when the LO is completely classical and deterministic.

Finally, compared to traditional balanced detections, since KKD is a direct detection scheme, it could be argued that it is robust to the phase noise [73] that is a major issue for traditional coherent detection scheme. However, we have shown that the LO still acts as a phase reference and therefore KKD should need phase stabilization of the LO in the case when it is not sent by the emitter. The impact of phase noise should still be different for KKD than for regular balanced detections and could be investigated.

Regarding the usage of an unbalanced beam splitter to mimic the sum described in Ref. [9], this could be avoided in the case where the signal of interest is a coherent state. Indeed, for a coherent state the sum could be generated at the source directly by using an optical IQ modulator. Alternatively, a wavelength division multiplexer could be used to sum the monochromatic part and the signal of interest without losing most of the LO power into the unmeasured output since the two are spectrally disjoint.

IV. KRAMERS-KRONIG PHASE OPERATOR

The phase operator defined via KKD signal processing is different from the phase operator of the quantum optics literature. Indeed, KKD phase operator is Hermitian and commutes with the intensity operator at time t (and not projected into a given mode). However, the quantum optics phase operator is not Hermitian and does not commute with the intensity. Besides, both phase and intensity operators are defined into a given temporal mode [47–51,53]. In this section, we investigate the phase information measured by KKD detection for some states of light such as bosonic coherent states, mixed states, and monomode pure states.

A. Bosonic coherent states

We start with a bosonic coherent state defined as

$$\begin{aligned}|[\psi]\rangle &= \exp\left\{\int_{-\infty}^{\infty} \mathrm{d}t\,\psi(t)\hat{c}^{\dagger}(t) - \mathrm{H.c.}\right\}|0\rangle \\ &= \exp\left\{\sqrt{\left(\int \mathrm{d}t\,|\psi(t)|^2\right)}\hat{c}^{\dagger}\left[\frac{\psi}{\sqrt{\int \mathrm{d}t\,|\psi(t)|^2}}\right]\right. \\ &\quad \left. - \mathrm{H.c.}\,|0\rangle\right\}. \end{aligned} \tag{26}$$

The bosonic coherent state [45,54,74] is intrinsically monomodal as it is possible to normalize the temporal distribution of the bosonic coherent state as it is done in the second equality. Under this form, the bosonic coherent state is a traditional coherent state where we precise the temporal or spectral mode of interest. It is, for example, the output state of a laser [74]. We assume $\psi(t) = A + \chi(t)$, where $\chi(t)$ is SSB and A is real and much larger than $\chi(t)$. Under these conditions, the phase of $\psi(t)$ is the Hilbert transform of the logarithm of its modulus. Such a state corresponds to the state of the measured output in Fig. 2(a), where the local oscillator state is a strong monochromatic coherent state, the input of interest state is a coherent state in an SSB mode, and the transmission of the beam splitter is close to 1 [75]. The characteristics of the beam splitter have been taken into account into A and $\chi(t)$ by rescaling and with the assumption that $A \gg \chi(t)$ for all t.

In order to calculate the moments of the intensity operator, one has to take into account the time response $h(t) \approx \delta(t)$ (or the bandwidth) of the photodiode, i.e., $\hat{I}(t) = \int_{-\infty}^{\infty} \mathrm{d}\tau h(t-\tau)\hat{c}^{\dagger}(\tau)\hat{c}(\tau)$. The response function should be close to a Dirac function compared to $\psi(t)$ at the first order. We then obtain

$$\begin{aligned}\langle[\psi]|\,\hat{I}(t)\,|[\psi]\rangle &= \int \mathrm{d}\tau h(t-\tau)|\psi(\tau)|^2 \approx |\psi(t)|^2, \\ \Delta^2_{|[\psi]\rangle}\hat{I}(t) &= \int \mathrm{d}\tau |h(t-\tau)|^2|\psi(\tau)|^2. \end{aligned} \tag{27}$$

The variance of the intensity for coherent bosonic states depends on the expectation value, similarly as the number operator for regular coherent states. However, it also depends on the time response of the photodiode. With the results of Appendix B, we calculate the first moment of the corresponding KKD phase operator:

$$\begin{aligned}\langle[\psi]|\,\hat{\varphi}_{\mathrm{KKD}}(t)\,|[\psi]\rangle &= -\mathcal{P}\int_{-\infty}^{\infty}\mathrm{d}t'\frac{\langle\hat{I}(t')\rangle - A^2}{A^2 2\pi(t-t')} + O\left(\frac{1}{A^2}\right) \\ &= -\mathcal{P}\int_{-\infty}^{\infty}\mathrm{d}t'\frac{\ln|\psi(t')|^2}{2\pi(t-t')} + O\left(\frac{1}{A^2}\right) \\ &= \arg\psi(t) + O\left(\frac{1}{A^2}\right), \end{aligned} \tag{28}$$

which matches the phase of the bosonic coherent state instantaneous amplitude. We remind that this phase is the relative phase since we have assumed the strong classical monochromatic LO to be real, setting the reference. Using the temporal response of the photodiode, the variance of the KKD phase

operator can be written as

$$\Delta^2\hat{\varphi}_{\mathrm{KKD}}(t) = \mathcal{P}\int_{-\infty}^{\infty} \mathrm{d}t'\,\mathrm{d}t''\,\mathrm{d}\tau\,\frac{h(t'-\tau)h(t''-\tau)|\psi(\tau)|^2}{\pi^2 A^4 (t-t')(t-t'')} + O\left(\frac{1}{A^3}\right) = O\left(\frac{1}{A^2}\right), \tag{29}$$

where for the second equality, we have used the fact that $|\psi(t)|^2$ is of order A^2 and $h(t)$ is of order 1. The stronger the monochromatic reference, the smaller the fluctuations in the measured phase of KKD become. This result is consistent as the phase of the field in the classical regime matches the KKD phase of strong bosonic coherent states.

B. Mixed states

We consider a mixture of bosonic coherent states

$$\hat{\rho} = \int \mathcal{D}^2[\psi] P[\psi]\,|[\psi]\rangle\langle[\psi]|\,, \tag{30}$$

where $\int \mathcal{D}[\psi] = \iint \mathcal{D}[\mathrm{Re}\{\psi\}]\mathcal{D}[\mathrm{Im}\{\psi\}]$ denotes a functional integral and $P[\psi]$ denotes a P-functional distribution [76,77] that contains the information on both the photon-number statistics and the spectral degree of freedom. For example, for a pure bosonic coherent state $|[\beta]\rangle$, $P[\alpha]$ is a Dirac functional distribution, i.e., $P[\alpha] = \delta([\alpha]-[\beta])$.

The measurement of the exact expectation value of KKD phase operator necessitates to measure all the moments of the intensity operator due to the high nonlinearity of the logarithm [see Eq. (21)]. In Appendix D, we show the expression of the first moments of the intensity operator for calculating the average value of the phase operator. We assume the state $\hat{\rho}$ to be a mixture of bosonic coherent states, all with the same monochromatic LO of amplitude A and an SSB signal with a small amplitude compared to the LO as in Sec. IV A. This state corresponds to the output of Fig. 2(a) when the LO is a pure strong monochromatic coherent state and the input $\hat{a}$ of interest is in a mixed state of SSB coherent state and the beam-splitter transmission coefficient is close to 1 [75]. The exact average value of the phase operator can be cast as $\langle\hat{\varphi}_{\mathrm{KKD}}(t)\rangle = \mathrm{tr}(\hat{\rho}\hat{\varphi}_{\mathrm{KKD}}(t))$:

$$\langle\hat{\varphi}_{\mathrm{KKD}}(t)\rangle = -\mathcal{P}\int \mathcal{D}[\psi]\mathrm{d}t' \sum_{1\leqslant l\leqslant k\leqslant n}^{\infty} \frac{P[\psi]}{2\pi(t-t')}\frac{(-1)^{n+k+1}}{n} \times \binom{n}{k}\left\{{k \atop l}\right\}\frac{|\psi(t')|^{2l}}{A^{2k}}, \tag{31}$$

where $\left\{{n \atop k}\right\} = \frac{1}{k!}\sum_{j=0}^{k}(-1)^{k-j}\binom{k}{j}j^n$ are the Stirling numbers of the second kind [78].

In the case of a pure bosonic coherent state $\hat{\rho} = |[\psi]\rangle\langle[\psi]|$ with a LO as well as an SSB signal in the same fashion as in Sec. IV A, the expectation value of KKD phase can be exactly written:

$$\langle\hat{\varphi}_{\mathrm{KKD}}(t)\rangle = -\mathcal{P}\int \sum_{1\leqslant l\leqslant k\leqslant n}^{\infty} \frac{\mathrm{d}t'}{2\pi(t-t')}\frac{(-1)^{n+k+1}}{n}\binom{n}{k}\left\{{k \atop l}\right\}\frac{|\psi(t')|^{2l}}{A^{2k}}, \tag{32}$$

which is an equivalent expression of the phase of the bosonic coherent state as developed in Eq. (28) at first order.

Now, in the case of an incoherent sum of bosonic coherent states $\hat{\rho} = \frac{1}{2}(|[\alpha]\rangle\langle[\alpha]| + |[\beta]\rangle\langle[\beta]|)$, keeping the hypothesis that both amplitudes of the bosonic coherent states are much smaller than the amplitude of the LO, the measured phase will be the sum of the relative phases between the local oscillator and each of the two SSB signals. For the most general mixed state, $\hat{\rho} = \sum_i p_i\,|[\psi]_i\rangle\langle[\psi]_i|$, which corresponds to the P-functional distribution $P[\psi] = \sum_i p_i\delta([\psi]-[\psi_i])$, the mean value of the measured phase would be the convex sum of all components of the mixture.

C. Pure monomode state

In this section, unlike the precedent sections, we consider the case of a LO with a nonzero phase to show that KKD determines the relative phase between the known local oscillator and the state of interest. This relative measured phase is composed of the particle-number statistics and the temporal mode structure of the state as we shall see.

We denote the state to be measured in the input $\hat{a}$ of the setup in Fig. 2(a) as

$$|\psi\rangle_a = \sum_{n=0}^{\infty} c_n\,|n\rangle_f = \sum_{n=0}^{\infty} c_n\frac{(\hat{a}^\dagger[f])^n}{\sqrt{n!}}\,|0\rangle\,, \tag{33}$$

where $\hat{a}^\dagger[f]$ is the creation operator associated with the mode f (see Appendix A for a precise definition) that is normalized, i.e., $\int_{-\infty}^{\infty}\mathrm{d}t|f(t)|^2 = 1$. By expressing the state in this manner, we factorize it into a product of a temporal component, represented by the mode function $f(t)$, and a particle-number degree of freedom, represented by the coefficients c_n. This factorization assumes the separability between the temporal mode $f(t)$ and the particle-number degree of freedom c_n, allowing us to treat them independently in the analysis. The direct detection in the output port $\hat{c}$ and in the temporal mode h can thus be expressed as

$$\hat{c}^\dagger[h]\hat{c}[h] = \tilde{t}^2\hat{a}^\dagger[h]\hat{a}[h] + \tilde{r}^2\hat{b}^\dagger[h]\hat{b}[h] + \tilde{t}\tilde{r}(\hat{a}^\dagger[h]\hat{b}[h] + \hat{b}^\dagger[h]\hat{a}[h]). \tag{34}$$

For an instantaneous measurement at time t, matching the one used for the photodiodes, we approximate the mode function $h(t')$ by $\delta(t-t')$. While the Dirac delta function $\delta(t-t')$ is not physically realizable as it cannot define a mode due to its lack of normalization, we use this approximation assuming that the detector's response time is much shorter than the temporal wave packet duration of the fields in input modes $\hat{a}$ and $\hat{b}$. The input of the beam splitter consists of the wavefunction of the state of interest in input mode $\hat{a}$ and a coherent state in input mode $\hat{b}$, used as a LO. This combined input state can be written as

$$|\psi\rangle_a\,|A_g\rangle_b = \left(\sum_{n=0}^{\infty} c_n\frac{(\hat{a}^\dagger[f])^n}{\sqrt{n!}}\right)\left(\sum_{n=0}^{\infty} e^{-\frac{|A|^2}{2}}\frac{A^n}{\sqrt{n!}}\frac{(\hat{b}^\dagger[g])^n}{\sqrt{n!}}\right)|0\rangle, \tag{35}$$

where f is the spectral mode associated with $\hat{a}$, g is the spectral mode associated with $\hat{b}$, and $|0\rangle$ is the vacuum state in

all input modes. Upon performing an instantaneous measurement, we obtain the following expression:

$$\begin{aligned}&\mathrm{tr}(\hat{c}^\dagger(t)\hat{c}(t)\,|\psi\rangle_a\,|A_g\rangle_b\,\langle\psi|_a\,\langle A_g|_b)\\&\quad=\tilde{t}^2|f(t)|^2\sum_{n=0}^{\infty}n|c_n|^2+\tilde{r}^2|A|^2|g(t)|^2\\&\qquad+\tilde{r}\tilde{t}f(t)g^*(t)A^*\sum_{n=0}^{\infty}c_nc_{n+1}^*\sqrt{n+1}+\mathrm{H.c.},\end{aligned}\tag{36}$$

where the last term is the interference term and couples both the state to be measured and the LO. For KKD, the LO is assumed to be known, constant, and strong with regard to the signal to be measured, which formally means that $g(t)=1$ up to an amplitude and a phase that can be taken into account in the symbol A. For practicality, we write $A=|A|e^{i\theta}$ where $|A|$ is the modulus and θ is the phase of the local oscillator. The state to be measured is SSB, which means that $f(t)$ is spectrally on the right of the carrier frequency as shown in Fig. 2(b). Under these conditions, the phase of the last term in Eq. (36) is reconstructed by KKD as it is possible to reconstruct the whole quantity. It includes the phase of the state of interest, which is $f(t)\sum_{n=0}^{\infty}c_nc_{n+1}^*\sqrt{n+1}$, comprising the phase of the spectral mode $\arg f(t)$ and the phase of the particle-number statistics $\arg\sum_{n=0}^{\infty}c_nc_{n+1}^*\sqrt{n+1}=\phi$. Therefore, the total measured phase here is

$$\zeta(t)=\theta-\phi+\arg f(t).\tag{37}$$

We now examine more specific examples. Consider the phase eigenstate whose wavefunction is

$$|\psi\rangle_a=(1-|z|^2)^{-1/2}\sum_{n=0}^{\infty}z^n\,|n\rangle_f\,,\tag{38}$$

with $z=|z|e^{i\phi}$ and $|z|<1$. This state is a normalizable eigenstate of the phase operator [47] (see Appendix C for a presentation), but is not an eigenstate of the phase operator measured with KKD [see Eq. (21)]. This example is specifically for justifying this difference between the two operators. For such a state, the phase detected with KKD yields for the interference term:

$$\begin{aligned}&Af(t)\sum_{n=0}^{\infty}c_nc_{n+1}^*\sqrt{n+1}\\&\quad=|A|e^{i\theta}f(t)z^*\frac{1}{1-|z|^2}\sum_{n=0}^{\infty}|z|^{2n}\sqrt{n+1}.\end{aligned}\tag{39}$$

Thus, we again obtain the relative phase $\zeta(t)=\theta-\phi+\arg f(t)$. Note that KKD is also effective for reconstructing the phase of superpositions of coherent states, such as the Schrodinger cat state, where the coefficients are given by $c_n=\frac{\alpha^n}{\sqrt{n!}}(1+(-1)^n)$.

V. SPECTRAL TOMOGRAPHY OF SINGLE PHOTONS INSPIRED BY KRAMERS-KRONIG DETECTION

In this section, we explore an alternative protocol inspired by KKD that allows for the complete characterization of both the temporal amplitude and phase of single-photon states, which uses spectral engineering. To achieve this, the total single-photon state must exist in a coherent superposition of two components: one that satisfies the SSB (spectral superposition) constraint and one that exhibits a quasimonochromatic spectrum. By combining these two elements, we can effectively capture the full temporal characteristics of the single-photon state. At the detection stage, instead of the PIN photodiode used for intensity measurements, a single-photon detector is employed. This substitution shifts the measurement from intensity to a probability distribution, which provides the necessary mathematical framework to recover the temporal phase of the single-photon state.

A. General idea

We start with a general single-photon state [44]:

$$|\psi\rangle=\hat{a}^\dagger[\psi]\,|0\rangle=\int_{-\infty}^{\infty}\mathrm{d}t\,\psi(t)\hat{a}^\dagger(t)\,|0\rangle\,,\tag{40}$$

where $\psi(t)$ denotes a normalized temporal mode. Similarly as in the bosonic coherent case, we consider $\psi(t)$ such that it verifies the Hilbert transform relation of Eq. (16):

$$\psi(t)=A+\chi(t),\tag{41}$$

where $A\gg|\chi(t)|$ for all t and $\chi(t)$, the unknown function to measure, is SSB. Theoretically, this state is not normalizable to 1 since the monochromatic A contribution has unbounded support. In practice, A should be replaced by $A\times\alpha(t)$, where $\alpha(t)$ is a temporal function of very large duration compared to $\chi(t)$ so that, compared to $\chi(t)$, it can be considered to be constant. It amounts to a function $\alpha(t)$ with localized spectrum. We stress that the total wavefunction should still be normalized and thus it is quasimonochromatic because $|A\alpha(t)|\gg|\chi(t)|$. In this context, the measured quantity is $p(t)=\langle\hat{a}^\dagger(t)\hat{a}(t)\rangle$, the probability of measuring a photon at time t on an ideal single-photon detector, and not the intensity measured by a photodiode. When $A\times\alpha(t)$ is assumed to be constant, the time-of-arrival distribution on an ideal single-photon detector is

$$p(t)=|\psi(t)|^2=|A+\chi(t)|^2.\tag{42}$$

The associated noise is not the vacuum quantum fluctuations anymore, but the noise due to the estimation of $p(t)$ with a finite number of measurements. The idea to reconstruct the phase is thus to plug the estimation of the probability distribution in KKD signal processing and reconstruct the phase of $\psi(t)$ that verifies the Hilbert transform relation:

$$\arg\psi(t)=-\mathcal{P}\int_{-\infty}^{\infty}\mathrm{d}t'\frac{\ln|\psi(t')|^2}{2\pi(t-t')},\tag{43}$$

where the integration limits are supposed to be infinite when the wavefunction verifies Eq. (41), that is to say when $\alpha(t)$ is almost constant. In practice, it means that the effective duration taken into account in the integral is smaller than the duration of $\alpha(t)$ and larger than the duration of $\chi(t)$. Now, the reconstructed phase converges to the phase of $\psi(t)$ as the number of measurements increases.

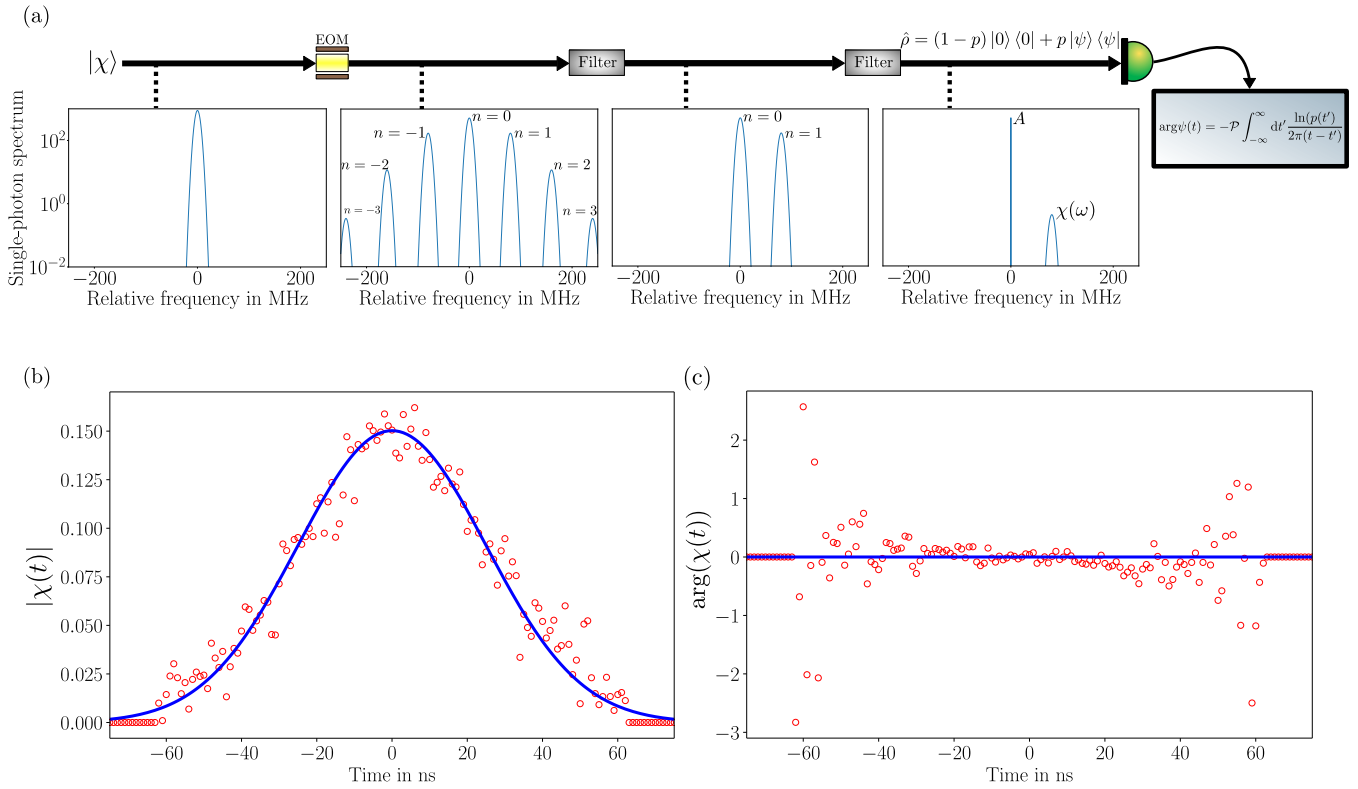


FIG. 4. (a) Setup for Kramers-Kronig spectral tomography of the single photon, (b) simulation results for the reconstruction of the modulus, and (c) simulation results for the reconstruction of the phase of a Gaussian wavefunction of bandwidth 40 MHz using Kramers-Kronig single-photon spectral tomography. Kramers-Kronig single-photon spectral tomography [panel (a)] consists first in performing signal engineering on the single photon of interest with the help of an electro-optic modulator and frequency filters. Below the setup, we show the evolution of the spectrum of a Gaussian at each step as an example. The result of the signal engineering is a coherent sum of a strong quasimonochromatic reference and the shifted wavefunction of interest. The resulting single-photon time-of-arrival distribution is measured with a single-photon detector. The probability undergoes Kramers-Kronig signal processing and the phase is reconstructed. The quasimonochromatic reference is filtered out and the wavefunction of interest is recovered. The simulated reconstruction [panels (b) and (c)] accounts for an electro-optic modulator modulated at 80 MHz with an efficiency of 20%. The monochromatic reference is created from the copy of order $n = 0$ with a low-pass filter of bandwidth 1 MHz. The single-photon detector simulated has a jitter time of 100 ps and a quantum efficiency of 40%. A dark count rate of 1 kHz for a sampling rate of 1 GHz has been taken into account. The plain (blue) curve corresponds to the target wavefunction and the round markers (red) correspond to the reconstructed wavefunction. The reconstruction reaches a fidelity of 96% for 10^8 simulated measurements.

B. Proposition of an experimental implementation

In this section, we propose a possible implementation of the KKD single-photon spectral tomography and more particularly of the spectral engineering necessary to turn a single-photon wavefunction $\chi(t)$ in the form of Eq. (41).

The setup proposed is shown in Fig. 4(a) and we show the spectrum of the single photon at each step for a Gaussian wavefunction as an example. We start with an on-demand or heralded single photon with temporal wavefunction $\chi(t)$. The bandwidth B of the single photon as well as the temporal duration T of the single photon are supposed to be known such that

$$\chi\left(t > \frac{T}{2}\right) \approx \chi\left(t < -\frac{T}{2}\right) \approx 0,$$
$$\mathcal{F}(\chi)\left(\omega > \frac{B}{2}\right) \approx \mathcal{F}(\chi)\left(\omega < -\frac{B}{2}\right) \approx 0. \tag{44}$$

The single photon goes through an EOM [64,79] that modulates the phase periodically with a sine function at frequency $\omega_{\mathrm{EOM}} > B$:

$$\chi_{\mathrm{EOM}}(t) = \chi(t)e^{-i\sin(\omega_{\mathrm{EOM}}t)} = \sum_{n=-\infty}^{\infty} e^{-in\omega_{\mathrm{EOM}}t} J_n(1)\chi(t). \tag{45}$$

Here, J_n denotes the Bessel functions of the first kind and we have used the Jacobi-Anger identity [80] to obtain the second line. The effect of the phase modulation in frequency is to repeat the spectral wavefunction of interest with the weight of each repetition defined by the Bessel functions of first order. Since $\omega_{\mathrm{EOM}} > B$, the copies do not overlap in frequency domain.

Then, we filter out all the repetitions but the ones for $n = 0$ that will serve as the quasimonochromatic reference and $n = 1$ that will serve as the SSB signal to reconstruct. In the case of an ideal filter of cutoff frequency $\omega_{\mathrm{min}} = -B/2$ and $\omega_{\mathrm{max}} \in [2\omega_{\mathrm{EOM}} - B/2, \omega_{\mathrm{EOM}} + B/2]$ localized between the copy of order $n = 1$ and $n = 2$, the input state is projected on the

subspace containing only the spectral contribution of the two first copies with probability $p_{\text{filter}} = |J_0(1)|^2 + |J_1(1)|^2 \approx 0.78$.

The single photon is filtered again in order to turn the copy of order $n = 0$ into a quasimonochromatic contribution (that plays the role of the LO in this protocol), leaving the $n = 1$ copy undistorted, which is the signal of interest. The filter for this only leaves a bandwidth $B_{\text{mono}} < B$ of the copy of order $n = 0$ and uniformly attenuates the copy $n = 1$ by a factor γ. As a rule of thumb, assuming that the distribution of the copy $n = 0$ of origin is evenly spread in the bandwidth B, the state after this second filtering is a mixed state that can be written as

$$\hat{\rho} = (1 - p)\,|0\rangle\langle 0| + p\,|\psi\rangle\langle\psi|\,, \tag{46}$$

composed of the vacuum $|0\rangle$ and a single photon $|\psi\rangle$ [whose temporal structure is now in the form of Eq. (41)] with probability

$$p = |J_0(1)|^2 \frac{B_{\text{mono}}}{B} + \gamma |J_1(1)|^2. \tag{47}$$

This second filter must be tight enough in frequency for the order $n = 0$ copy to be considered constant in time compared to the $n = 1$ copy and could be performed with a wave shaper. The attenuation of the repetition $n = 1$ must be enough for the quasimonochromatic reference to be stronger than the repetition $n = 1$, to verify the MP constraint. The single-photon time-of-arrival density probability distribution is measured with a single-photon detector with timing jitter T_{jit}. As a result, the time-of-arrival density probability distribution is sampled at period t_s larger than the jitter time and only approximately T/t_s histogram points are relevant for the reconstruction.

Finally, the reconstructed probability of time of arrival undergoes KKD signal processing. The quasimonochromatic reference is filtered out with a digital high-pass filter and the initial wavefunction of interest is reconstructed.

The first limitations of KKD single-photon spectral tomography regarding the class of single-photon wavefunctions [81–83] that can be reconstructed concern the bandwidth and the duration of the wave packet. The bandwidth B of the single photon is limited by the modulation speed of the EOM, which should be large enough to shift the wavefunction in frequency without causing overlaps. Bandwidths of EOM reach several gigahertz in the literature [63–66]. The duration T of the single photon is limited by the timing jitter of the single-photon detector, which should be low enough to have enough samples per pulse for KKD digital signal processing to be efficient. The timing jitter of current single-photon detectors reaches the picosecond scale in the literature [84–87]. Finally, another constraint is the dark count rate of the single-photon detector that must largely lower bound the repetition rate of the experiment such that only a low number of parasitic counts are detected compared to the single-photon events. Current single-photon detectors reach dark count rates at the hertz level [85,88]. For each single-shot measurement, the probability of success is upper bounded by Eq. (47) in the ideal lossless case without dark counts.

In Figs. 4(b) and 4(c), we show a simulation of the reconstruction using our setup idea (see Appendix E for a detailed explanation). The extra losses due to the EOM as well as the single-photon detector efficiency are taken into account. A fidelity of 96% is reached with 10^8 simulated measurements. The wavefunction to reconstruct is a Gaussian of characteristic bandwidth 40 MHz that corresponds to a duration of $T \approx 100$ ns, where 98% of the time-of-arrival distribution of the Gaussian wavefunction of the single photon is contained in $[-\frac{T}{2}, \frac{T}{2}]$:

$$\int_{-\frac{T}{2}}^{\frac{T}{2}} \mathrm{d}t\,|\chi(t)|^2 \approx 0.98, \tag{48}$$

where $\chi(t)$ is the wavefunction of interest. The simulated EOM is lossy with an efficiency of 20% and a modulation frequency of 80 MHz. The filtering process only keeps a centered 1 MHz bandwidth from the $n = 0$ repetition. For this value of bandwidth for the quasimonochromatic reference, an attenuation of 0.04 has been applied on the $n = 1$ repetition. Finally, a lossy single-photon detector of efficiency 40% with a dark count rate of 1 kHz and a jitter time of 100 ps has been simulated. For a sampling period $t_s = 1$ ns, we have $T/t_s = 100$ bins in the histogram per pulse. These performances should be reachable for state-of-the-art avalanche photodiode (APD) single-photon detectors. Other examples of single-photon wavefunction reconstruction, Gaussian and coherent superposition of two Gaussians, with different modulus and different phases can be found in Appendix E. With one APD detector, we found a fidelity higher than 95% for the reconstruction.

Compared to other protocols in the literature based on shearing and frequency-resolved single-photon detectors [55–61], the described protocol relies on spectral engineering and time-resolved single-photon detectors. Given the state-of-the-art regarding single-photon detectors and EOMs, the described protocol could be used for the spectral tomography of narrowband single photons with long coherence time emitted by, e.g., atomic Rubidium clouds [83] or single atoms [81,82] with a bandwidth shorter than that of the single-photon detectors. The EOM in our protocol enables coherent summation of two spectrally disjoint components required for KK signal processing. However, the EOM introduces an inherent minimum loss due to modulation and filtering of unused sidebands. Using sinusoidal phase modulation, sidebands are generated with amplitudes given by Bessel functions of the first kind. When the modulation frequency is high enough to avoid spectral overlap, filtering out all replicas except $n = 0$ and $n = 1$ retains approximately 78% of the original energy, corresponding to a minimum loss of 22%, excluding injection losses.

For comparison, we emphasize on two examples. The first is a shearing interferometry experiment [57] that reports total losses of 40%, mainly due to grating inefficiency and fiber coupling losses. Finally, an alternative to perform the coherent sum of the monochromatic contribution and the wavefunction of interest is to employ an alternating sequence of EOMs and wave shapers as presented in Ref. [89]. While the gate fidelity is close to 1, the injection losses are important, 3 dB for each optical element.

VI. CONCLUSION

We have performed the quantization of the KKD detection and calculated the first two moments of the intensity and phase measured operators with the hypothesis of ideal optics, ideal signal processing, and classical LO. We have shown that KKD is a Gaussian measurement at the first order in the LO, meaning that it measures both quadratures of quantum fields at the first order in the LO. We have also pointed out that KKD yields the same quantum fluctuations as DHD. This detection protocol reconstructs the phase of a quantum state from a direct intensity measurement; however, we stress that the measured KKD phase operator is not the phase operator defined in the quantum optics literature. We have illustrated that the phase reconstruction procedure works in particular for bosonic coherent states and mixture of coherent bosonic states, and for monomode pure states. A phase that depends on both the spectral degree of freedom of the mode and the photon-number statistics can also be reconstructed.

Alternatively, we have shown that a protocol based on KKD may be used to perform the spectral tomography of single-photon states. This estimation of the temporal wave packet relies on temporally resolved single-photon detectors and spectral engineering.

Furthermore, as a direct detection, KKD shifts the optical complexity of traditional balanced detection into signal processing complexity [3,17]. It would mean that KKD is immune from sources of technical noise related to finite common mode rejection ratio that may limit the performance of quadrature measurement with a balanced coherent receiver, for example [90]. In regular balanced detections, this issue has to be solved in the optical and electrical domain by fine-tuning the experimental setup [39] to the balanced photodiodes or the beam splitters. Finally, direct detection alternatives to KKD, based on iterative algorithms and dispersion, for example, have been proposed in the field of classical telecommunications [17,91–93]. In the classical regime, they act as coherent detectors but their validity could also be investigated in the quantum regime.

ACKNOWLEDGMENTS

T.P. acknowledges funding from IMT, l'Institut Carnot TSN, and the Fondation Mines-Télécom. This project has received funding from the European Union's Horizon Europe research and innovation programme under the project "Quantum Secure Networks Partnership" (QSNP, Grant Agreement No. 101114043). We are also very grateful for fruitful discussions with Elie Awwad.

DATA AVAILABILITY

The data are available from the authors upon reasonable request. The code for single-photon tomography has been deposited in Ref. [94].

APPENDIX A: FIELD QUANTIZATION AND CORRESPONDENCE PRINCIPLE

In this Appendix, we recall the basics of the electromagnetic field quantization that we used to construct the quantum KKD detection from its classical equivalent. We will stress the main steps and results, but a more detailed approach can be found, e.g., in Refs. [95,96]. The quantization procedure follows a sequence of steps: (1) Starting from Maxwell's equations written in a Hamiltonian form and providing a pair of canonical variables. (2) A classical complex Hilbert space $\mathcal{H}$ is built such that it represents the Hamiltonian structure. (3) A bosonic Fock space $\mathcal{F}(\mathcal{H}) = \bigoplus_{n=0}^{\infty} \mathcal{H}^{\otimes_S n}$ is constructed, where $\mathcal{H}^{\otimes_S n}$ is the symmetrized n-times tensor product of $\mathcal{H}$ with itself. Each subspace for a fixed n corresponds then to the subspace of n-photon states. The passage from one subspace to another is done using bosonic creation-annihilation operators $\hat{a}^\dagger[\psi]$ and $\hat{a}[\psi]$, defined directly for any element $\psi \in \mathcal{H}$, and satisfying the standard bosonic commutation relations $[\hat{a}[\psi], \hat{a}^\dagger[\phi]] = \langle \psi, \phi \rangle_{\mathcal{H}}$ [44,45,96]. (4) The construction of quantum observables is performed using a correspondence principle, initially guided by the harmonic-oscillator-like form of the electromagnetic field Hamiltonian. (5) The definition of the generator of the quantum dynamics in Fock space is deduced from the single-photon dynamics, itself determined by the classical Hamiltonian dynamics.

In our case, since we use passive optical elements like beam splitters, one has to consider Maxwell's equations in an inhomogeneous passive dielectric medium characterized by its position-dependent dielectric function. It has been shown (see, e.g., the pioneering work [95] or more recent contributions [96–98]) that a treatment identical to that of the vacuum can be done, the only difference being that the generator of the dynamics will automatically include the medium properties. Therefore, any real classical field $F(x)$ that can be written in terms of a basis of valid initial conditions for Maxwell's equations, i.e., for any $\{\varphi_\kappa(x)\} \in \mathcal{H}$ as

$$F(x) = \sum_\kappa z_\kappa \varphi_\kappa(x) + \text{c.c.}, \tag{A1}$$

where $z_\kappa = \langle \varphi_\kappa \rangle F_{\mathcal{H}}$, will be quantized through the following correspondence principle: $z_\kappa \mapsto \hat{a}[\varphi_\kappa]$ and $z_\kappa^* \mapsto \hat{a}^\dagger[\varphi_\kappa]$, which yields the quantum observable

$$\hat{F}(x) = \sum_\kappa \hat{a}[\varphi_\kappa]\varphi_\kappa(x) + \text{H.c.} \tag{A2}$$

We emphasize that κ represents here a possible combination of continuous and discrete indices that correspond to the spectrum degeneracy of the considered system. In particular, one could take, in free space, the basis of circularly polarized plane waves for which $\kappa \equiv (\vec{k}, \sigma)$, where $\vec{k}$ is the wave vector and σ denotes the two possible polarizations; for this case, the sum over κ in fact hides $\sum_\kappa \equiv \int_{\mathbb{R}^3} d^3k \sum_{\sigma=\pm}$.

Similarly as the creation and annihilation operators, to each solution of the Maxwell's equations we associate two hermitian operators called the quadratures:

$$\hat{q}_a[\psi] = \frac{\hat{a}[\psi] + \hat{a}^\dagger[\psi]}{2},$$
$$\hat{p}_a[\psi] = \frac{\hat{a}[\psi] - \hat{a}^\dagger[\psi]}{2i}. \tag{A3}$$

They follow the canonical position/momentum commutation relations $[\hat{q}_a[\psi], \hat{p}_a[\phi]] = \frac{i}{2}\text{Re}\{\langle\psi\rangle \phi_{\mathcal{H}}\}$, $[\hat{q}_a[\psi], \hat{q}_a[\phi]] = [\hat{p}_a[\psi], \hat{p}_a[\phi]] = \frac{i}{2}\text{Im}\{\langle\psi\rangle \phi_{\mathcal{H}}\}$. In our convention, the

quadratures are the analog of the real part and the imaginary part of the field in a specified mode that explains the factor 2 in Eq. (A3) instead of $\sqrt{2}$.

By construction, Maxwell's equations relate vectorial quantities that depend both on time and on the three dimensions of space. However, here we did not specify the vectorial dependence since it does not affect the quantization and the coherent detection problems we want to treat can be reduced to one-dimensional situations. We consider a propagating one-dimensional field in the $+x$ direction. The only degree of liberty left is the wave vector $k_x \geqslant 0$, along the propagating direction. We apply the change of variable $t = x/c$ and $\omega = c|k_x|$, where the time t is the detection time of the photodiode and ω is the frequency associated with the spectrum of the signal. In the context of optical telecom communications, we consider only wave packets located around a carrier frequency (typically 1550 nm). These wavefunctions have low bandwidth compared to the carrier frequency. Formally, it means that we consider wavefunctions of the form $\psi(t) = C \times e^{-i\omega_c t} f(t)$, where $f(t)$ bandwidth is very small with regard to ω_c the carrier frequency. The constant C being the same for all the family of mode f, we consider so that all modes f are normalized to 1. In this context, we will denote $\hat{a}[f]$ and $\hat{a}^\dagger[f]$ instead of $\hat{a}[\psi]$ and $\hat{a}^\dagger[\psi]$, the frequency shift being implicit. The inner product used in the commutation relations associated with the considered Hilbert space of modes becomes $\langle f|g\rangle_{\mathcal{H}} = \int_{-\infty}^{\infty} \mathrm{d}t\, f^*(t)g(t)$. Considering a family of wavefunction f_κ, we can write the electric field at time t:

$$\hat{E}(t) = Ce^{-i\omega_c t} \sum_\kappa \hat{a}[f_\kappa] f_\kappa(t) + \text{H.c.} \tag{A4}$$

Useful operators are the annihilations and creation operators at time t: $\hat{a}(t) = \sum_\kappa \hat{a}[f_\kappa] f_\kappa(t)$ and $\hat{a}^\dagger(t) = \sum_\kappa \hat{a}^\dagger[f_\kappa] f_\kappa^*(t)$, where κ spans over all possible modes. For any mode f, one can express $\hat{a}[f]$ and $\hat{a}^\dagger[f]$ as a function of $\hat{a}(t)$ and $\hat{a}^\dagger(t)$:

$$\begin{aligned} \hat{a}[f] &= \int_{-\infty}^{\infty} \mathrm{d}t\, f^*(t)\hat{a}(t), \\ \hat{a}^\dagger[f] &= \int_{-\infty}^{\infty} \mathrm{d}t\, f(t)\hat{a}^\dagger(t). \end{aligned} \tag{A5}$$

In particular, one can define for practical purposes the annihilation/creation operators associated with plane waves at frequency $\omega_c + \omega$:

$$\begin{aligned} \hat{a}(\omega) &= \int_{-\infty}^{\infty} \mathrm{d}t\, e^{i\omega t}\hat{a}(t), \\ \hat{a}^\dagger(\omega) &= \int_{-\infty}^{\infty} \mathrm{d}t\, e^{-i\omega t}\hat{a}^\dagger(t), \end{aligned} \tag{A6}$$

with the inverse transform being

$$\begin{aligned} \hat{a}(t) &= \mathcal{F}^{-1}(\hat{a})(t) = \int_{-\infty}^{\infty} \frac{\mathrm{d}\omega}{2\pi} e^{-i\omega t}\hat{a}(\omega), \\ \hat{a}^\dagger(t) &= \int_{-\infty}^{\infty} \frac{\mathrm{d}\omega}{2\pi} e^{i\omega t}\hat{a}^\dagger(\omega), \end{aligned} \tag{A7}$$

where we extended ω (frequency relative to the carrier) to $-\infty$ for convenience regarding the commutation relations. We stress that ω is a relative frequency, hence the possible negativity. In practice, it means that the considered states are localized around the carrier frequency so that $\omega \to -\infty$ and $\omega \to \infty$ plane waves are never populated. With continuous parametrization t or ω, the operators have to be seen as distribution and their commutation relations yield Dirac distributions [44]: $[\hat{a}(t), \hat{a}^\dagger(t')] = \delta(t - t')$ and $[\hat{a}(\omega), \hat{a}^\dagger(\omega')] = \delta(\omega - \omega')$.

Finally, we can define the quadrature operators at time t:

$$\begin{aligned} \hat{q}(t) &= \frac{\hat{a}(t) + \hat{a}^\dagger(t)}{2}, \\ \hat{p}(t) &= \frac{\hat{a}(t) - \hat{a}^\dagger(t)}{2i}. \end{aligned} \tag{A8}$$

APPENDIX B: KRAMERS-KRONIG SIGNAL PROCESSING

In this Appendix, we show that the measurement of the intensity leads to the measurement of the phase in the quantum regime from Sec. III. We write the input of the photodiode of Fig. 2(a):

$$\tilde{r}\hat{b}(t) + \tilde{t}\hat{a}(t) = \tilde{r}A + \tilde{t}\hat{q}(t) + i\tilde{t}\hat{p}(t). \tag{B1}$$

When calculating the photocurrent at the output of the photodiode, we have the quadratic term of the local oscillator, the quadratic term of the signal, and cross terms with the signal and the local oscillator. These cross terms filter out the momentum quadrature of the signal. Next, we suppose that $\tilde{r}$ and $\tilde{t}$ are real since the phase could be accounted for by a rotation of the phase space of $\hat{a}$. The intensity of the photodiode writes

$$\hat{I}(t) = \tilde{r}^2 A_0^2 + 2\tilde{t}\tilde{r}A\hat{q}_\theta(t) + \tilde{r}^2\hat{a}^\dagger(t)\hat{a}(t), \tag{B2}$$

where $\hat{q}_\theta(t)$ correspond to the quadrature in time of $\hat{a}(t)e^{-i\theta}$ and the last term is negligible with regard to the other two because of the local oscillator amplitude and the amplitudes of the signal states under study. To calculate the Hilbert transform of the intensity, one needs to write the logarithm of the intensity as an operator. To do so, we use a perturbative approach. The intensity of the field at the input of the photodiode is equal to zero order to $\tilde{r}^2 A_0^2$.

$$\begin{aligned} \ln \hat{I}(t) &= \ln \tilde{r}^2 A_0^2 \left(1 + \frac{\hat{I}(t) - \tilde{r}^2 A_0^2}{\tilde{r}^2 A_0^2}\right) \\ &= \ln \tilde{r}^2 A_0^2 + \sum_{n=1}^{\infty} \frac{(-1)^{n+1}}{n} \left(\frac{\hat{I}(t) - \tilde{r}^2 A_0^2}{\tilde{r}^2 A_0^2}\right)^n \\ &= \ln \tilde{r}^2 A_0^2 + \frac{\hat{I}(t) - \tilde{r}^2 A_0^2}{\tilde{r}^2 A_0^2} + O\left(\frac{1}{A_0^2}\right), \end{aligned} \tag{B3}$$

where $O(1/A_0^2)$ denotes an operator whose expectation value for the considered states is on the order of $O(1/A_0^2)$. Using the fact that Cauchy's principal value acting on odd functions yields zero, the decomposition in frequency components of the field operator (see Appendix A), and Dirichlet's integral $\int_{-\infty}^{\infty} \mathrm{d}x \sin x/x = \pi$, we calculate the phase operator defined

by KKD:

$$\begin{aligned}
\hat{\varphi}_{\mathrm{KKD}}(t) &= -\mathcal{P}\int_{-\infty}^{\infty} \mathrm{d}t' \frac{\hat{I}(t') - \tilde{r}^2 A_0^2}{\tilde{r}^2 A_0^2} \times \frac{1}{2\pi(t-t')} + O\left(\frac{1}{A_0^2}\right) \\
&= -\mathcal{P}\int_{-\infty}^{\infty} \mathrm{d}t' \frac{\tilde{t}}{\tilde{r}} \frac{\hat{a}(t-t')e^{-i\theta} + \hat{a}(t-t')e^{i\theta}}{2A_0\pi t'} + O\left(\frac{1}{A_0^2}\right) \\
&= -\mathcal{P}\int_{-\infty}^{\infty} \mathrm{d}t' \int_{-\infty}^{\infty} \frac{\mathrm{d}\omega}{2\pi} \left\{ \frac{\tilde{t}}{\tilde{r}} \frac{\hat{a}_\theta(\omega)e^{-i\omega(t-t')}}{2A_0\pi t'} + \frac{\hat{a}_\theta^\dagger(\omega)e^{i\omega(t-t')}}{2A_0\pi t'} \right\} + O\left(\frac{1}{A_0^2}\right) \\
&= -\mathcal{P}\int_{-\infty}^{\infty} \mathrm{d}t' \int_{-\infty}^{\infty} \frac{\mathrm{d}\omega}{2\pi} \frac{\tilde{t}}{\tilde{r}} \left\{ \frac{\hat{q}_\theta(\omega)\cos(\omega(t-t'))}{A_0\pi t'} + \frac{\hat{p}_\theta(\omega)\sin(\omega(t-t'))}{A_0\pi t'} \right\} + O\left(\frac{1}{A_0^2}\right) \\
&= \mathcal{P}\int_{-\infty}^{\infty} \mathrm{d}t' \int_{0}^{\infty} \frac{\mathrm{d}\omega}{2\pi} \frac{\tilde{t}}{\tilde{r}} \left\{ \frac{(\hat{p}_\theta(\omega) - \hat{p}_\theta(-\omega))\cos\omega t \sin\omega t'}{A_0\pi t'} - \frac{(\hat{q}_\theta(\omega) + \hat{q}_\theta(-\omega))\sin\omega t \sin\omega t'}{A_0\pi t'} \right\} + O\left(\frac{1}{A^2}\right) \\
&= \int_{0}^{\infty} \frac{\mathrm{d}\omega}{2\pi} \frac{\tilde{t}}{\tilde{r}} \left\{ \frac{(\hat{p}_\theta(\omega) - \hat{p}_\theta(-\omega))\cos\omega t}{A} - \frac{(\hat{q}_\theta(\omega) + \hat{q}_\theta(-\omega))\sin\omega t}{A} \right\} + O\left(\frac{1}{A^2}\right).
\end{aligned} \tag{B4}$$

To go from the fourth equality to the fifth, we used the fact that $\cos(\omega t')/t'$ is odd in t' and thus yields a zero Cauchy principal value, and we wrote the integral over $(-\infty, \infty)$ as a sum of integral over $(0, \infty)$. And to go from the fifth equality to the sixth, we used the fact that $\int \sin(\omega t')/t' \mathrm{d}t' = \mathrm{sign}(\omega) \times \pi$.

We reconstruct $\hat{a}(t)$ using $\hat{\varphi}_{\mathrm{KKD}}(t)$ and the measured intensity:

$$\begin{aligned}
\hat{a}_{\mathrm{KKD}}(t) &= \frac{e^{i\hat{\varphi}_{\mathrm{KKD}}(t)}\sqrt{\hat{I}(t)} - \tilde{r}A_0}{\tilde{t}} \\
&= \frac{\tilde{r}}{\tilde{t}}A_0(1 + i\hat{\varphi}_{\mathrm{KKD}}(t))\left(1 + \frac{\tilde{t}}{\tilde{r}}\frac{\hat{q}(t)}{A_0}\right) - \frac{\tilde{r}}{\tilde{t}}A_0 + O\left(\frac{1}{A_0}\right) \\
&= \int_0^\infty \frac{\mathrm{d}\omega}{2\pi} \{(\hat{q}_\theta(\omega) + \hat{q}_\theta(-\omega))e^{-i\omega t} + i(\hat{p}_\theta(\omega) - \hat{p}_\theta(-\omega))e^{-i\omega t}\} + O\left(\frac{1}{A_0}\right) \\
&= \int_0^\infty \frac{\mathrm{d}\omega}{2\pi} (\hat{a}_\theta(\omega)e^{-i\omega t} + \hat{a}_\theta^\dagger(-\omega)e^{-i\omega t}) + O\left(\frac{1}{A_0}\right),
\end{aligned} \tag{B5}$$

where the equality is written to first order in $1/A_0$ and where the square root has been calculated with a Taylor expansion similar to the logarithm in Eq. (B3): $\sqrt{\hat{I}(t)} = \tilde{r}A_0\sqrt{1 + \frac{\hat{I}(t) - \tilde{r}^2A_0^2}{\tilde{r}^2A_0^2}}$. We stress that the $\hat{a}_{\mathrm{KKD}}(t)$ operator is not a bosonic annihilation operator as it does not follow the canonical commutation relations.

For a given mode $f(t) = \int_0^\infty \frac{\mathrm{d}\omega}{2\pi}\mathcal{F}(f)(\omega)e^{-i\omega t}$ single sideband, we can estimate $\hat{a}[f]$:

$$\begin{aligned}
\hat{a}[f]_{\mathrm{KKD}} &= \int_{-\infty}^{\infty} \mathrm{d}t\, f^*(t)\hat{a}_{\mathrm{KKD}}(t) \\
&= \int_0^\infty \frac{\mathrm{d}\omega}{2\pi}\mathcal{F}(f)(\omega)^*\hat{a}(\omega) \\
&\quad + \int_0^\infty \frac{\mathrm{d}\omega}{2\pi}\mathcal{F}(f)(\omega)^*\hat{a}^\dagger(-\omega) + O\left(\frac{1}{A_0}\right) \\
&= \hat{a}[f] + \hat{a}^\dagger[f^*] + O\left(\frac{1}{A_0}\right),
\end{aligned} \tag{B6}$$

where $\hat{a}[f]_{\mathrm{KKD}}$ is the estimator. We used Parseval identity for the second equality and the fact that $\mathcal{F}(f^*)(\omega) = \mathcal{F}(f)(-\omega)^*$ for the last equality. The quadratures are reconstructed as the hermitian and anti-hermitian parts of $\hat{a}[f]_{\mathrm{KKD}}$ and we find the result of Eq. (24).

APPENDIX C: PHASE AND NUMBER OPERATORS

In Eq. (23), we used the KKD phase operator as if it was the phase from the polar decomposition of the annihilation operator at the output of the beam splitter $\hat{c}(t)$, but it is not since it commutes with the intensity operator. In this Appendix, we remind the expression of what is called the phase operator in the quantum optics literature, as well as its eigenstate [47,48,51,52], to highlight the differences with the phase measured by KKD.

We consider the generic quantum harmonic oscillator, where the ladder operators (also called creation and annihilation operators) can be written as a polar decomposition as proposed by Susskind and Glogover [47,48,52]:

$$\hat{a}^\dagger = \hat{n}^{1/2}\hat{E}_+ = \hat{E}_+(\hat{n}+1)^{1/2}, \tag{C1}$$

$$\hat{a} = (\hat{n}+1)^{1/2}\hat{E}_- = \hat{E}_-\hat{n}^{1/2}, \tag{C2}$$

where

$$\hat{E}_- = \sum_{n=0}^{\infty} |n\rangle \langle n+1|, \tag{C3}$$

$$\hat{E}_+ = \sum_{n=0}^{\infty} |n+1\rangle\langle n|. \tag{C4}$$

We have $\hat{E}_\pm^\dagger = \hat{E}_\mp$; thus, the operators are not hermitian and are therefore not observables. The expectation value can still be obtained if the full tomography is performed. They should be understood as the complex exponentials of the phase operator even though they are not unitary and thus cannot be mathematically written as complex exponentials. Further, cosine and sine phase operators can be defined: $\hat{C} = 1/2(\hat{E}_- + \hat{E}_+)$ and $\hat{D} = 1/(2i)(\hat{E}_- - \hat{E}_+)$, and they are called in such a way since they reproduce the same algebraic structure as the projections of the classical harmonic oscillator state in phase space; however, one must be careful as they do not commute since the $\hat{E}_\mp$ operators are not exponentials. Also $\hat{C}$ and $\hat{D}$ are hermitian and therefore are observables. Note that we have the inverse relation:

$$\hat{E}_+ = \frac{1}{\sqrt{\hat{n}}}\hat{a}^\dagger, \quad \hat{E}_- = \hat{a}\frac{1}{\sqrt{\hat{n}}}. \tag{C5}$$

The phase displacement operator can be defined as

$$\hat{D}(\phi) = e^{i\phi\hat{n}} \tag{C6}$$

and is unitary. The number displacement operator built from the exponential of the phase operator (increasing and decreasing, respectively, of n steps),

$$\hat{\mathcal{D}}^-(n) = \hat{E}_-^n, \quad \hat{\mathcal{D}}^+(n) = \hat{E}_+^n, \tag{C7}$$

is not unitary but isometric only since the vacuum state does not have a preimage. This is a consequence of having a half-discrete line for the levels of energy.

One can check that

$$[\hat{n}, \hat{E}_+] = \hat{E}_+, \quad [\hat{E}_-, \hat{n}] = \hat{E}_-, \quad [\hat{E}_+, \hat{E}_-] = |0\rangle\langle 0|, \tag{C8}$$

which is therefore different than the $e(2)$ algebra due to the "cut," and we have $\hat{E}_-\hat{E}_+ = \mathbb{I}$. The Fock state forms a completeness relation: $\sum_{n\in\mathbb{N}} |n\rangle\langle n| = \mathbb{I}$. They are the eigenstates of the number operator $\hat{n}|n\rangle = n|n\rangle$, which can be written as $\hat{n} = \sum_{n=0}^{\infty} n|n\rangle\langle n|$.

A correct (normalizable) eigenstate of the exponential of the phase operator $\hat{E}_-$, $\hat{E}_-|z\rangle = z|z\rangle$ is defined as follows [48,52]:

$$|z\rangle = (1-|z|^2)^{-1/2}\sum_{n=0}^{\infty} z^n |n\rangle, \tag{C9}$$

with $|z| < 1$. Note that the mode structure is implicit in the notation $|n\rangle$ that should be read as $|n\rangle_\psi$. Finally, the phase state can appear as a coherent state in a truncated Fock space [99]. Another approach is the Pegg and Barnett formalism [51] where the Fock space is truncated up to a maximum number of excitations, and the limit toward infinity is taken at the end of every expectation value calculation. If $|z| = 1$, the state is not normalizable: It would be convenient to have such a form as a Fourier series, but this is not the case. The truncated phase eigenstate can be written as $|\phi\rangle = (\frac{1}{s+1})^{1/2}\sum_{n=0}^{s} e^{i\phi n}|n\rangle_\psi$, from which we do not have constraints on the radius anymore for having a normalized state. Notice that if one takes the limit $s \to \infty$, the state is not normalizable anymore and corresponds to the eigenstate mentioned in Refs. [47,48].

The phase operator introduced in this paper necessary commutes with the number operator as $\hat{\varphi}_{\mathrm{KKD}}(t)$ is a function of $\hat{n}(t)$:

$$[\hat{n}(t'), \hat{\varphi}_{\mathrm{KKD}}(t)] = 0, \tag{C10}$$

and even after integrating over time, $\hat{\varphi}_{\mathrm{KKD}}(t)$ is not the logarithm of $\hat{E}_\pm$ because it is not well defined as it is singular. Therefore, the eigenstate of the exponential of the phase operator $\hat{E}$ is not the one of $\hat{\varphi}_{\mathrm{KKD}}(t)$.

Another naive attempt to define a phase operator would be by adding a filtering function $v(t)$ as it is done for the annihilation operator:

$$\begin{aligned}\hat{\varphi}_{\mathrm{KKD}}[v] &= \int \mathrm{d}t\, v(t)\hat{\varphi}_{\mathrm{KKD}}(t)\\ &= \iint \mathrm{d}t\,\mathrm{d}t' \frac{1}{\pi(t-t')} v(t)\ln(\hat{I}(t'))\\ &= \int \mathrm{d}t' f(t')\ln(\hat{I}(t')) = \ln(\hat{I})[f],\end{aligned} \tag{C11}$$

where $f(t') = \int \mathrm{d}t \frac{v(t)}{2\pi(t-t')}$. However, it is certain that it cannot respect the relation $[\hat{n}, e^{i\hat{\varphi}_{\mathrm{KKD}}}] = e^{i\hat{\varphi}_{\mathrm{KKD}}}$ as in Eq. (C8). Indeed, in Eq. (C11), the phase and the intensity are projected into different modes.

APPENDIX D: AVERAGE VALUE OF THE PHASE OPERATOR WITH RESPECT TO MIXED STATE

In this Appendix, we present the main calculations for obtaining the expression of the average value of the phase measured with KKD, from the moments of the direct intensity operator. The expectation value of the instantaneous intensity operator is

$$\mathrm{Tr}(\hat{\rho}\hat{a}^\dagger(t)\hat{a}(t)) = \iint \mathcal{D}[\alpha]\mathcal{D}[\beta]P[\alpha]|\langle[\beta]\rangle\,[\alpha]|^2\alpha^*(t)\beta(t), \tag{D1}$$

where we have used the completeness relation of the bosonic coherent state $\int \mathcal{D}[\alpha]\,|[\alpha]\rangle\langle[\alpha]| = \mathbb{I}$. The scalar product is $|\langle[\beta]\rangle\,[\alpha]|^2 = \exp(-\int \mathrm{d}t|\beta(t)-\alpha(t)|^2)$ (see Refs. [54,100]). The integration over β leads to

$$\int \mathcal{D}[\beta]\exp\left(-\int \mathrm{d}t'|\beta(t')-\alpha(t')|^2\right)\beta(t) = \alpha(t), \tag{D2}$$

where to perform the functional integral, we can perform the derivative with respect to $\alpha^*(t)$ or by using a change of variable. Finally, we obtain

$$\mathrm{Tr}(\hat{\rho}\hat{a}^\dagger(t)\hat{a}(t)) = \int \mathcal{D}[\alpha]P[\alpha]|\alpha(t)|^2. \tag{D3}$$

The average value of the phase obtained with KKD puts into play the expression of the logarithm of the intensity, logarithm that is expanded into a power series, with respect to a strong local oscillator. Thus, every moment of the intensity operator appears. We have, for instance,

$$\mathrm{Tr}(\hat{\rho}(\hat{a}^\dagger(t)\hat{a}(t))^2) = \int \mathcal{D}[\alpha]P[\alpha](|\alpha(t)|^4 + |\alpha(t)|^2). \tag{D4}$$

Using the result of Ref. [78] for the nth power, we compute the logarithm of the intensity operator:

$$\begin{aligned}
&\mathrm{Tr}\{\hat{\rho}\ln\hat{a}^\dagger(t)\hat{a}(t)\}\\
&= \ln A^2 + \sum_{n=0}^{\infty}(-1)^{n-1}\frac{\mathrm{Tr}\{\hat{\rho}(\hat{a}^\dagger(t)\hat{a}(t)-A^2)^n\}}{nA^{2n}}\\
&= \ln A^2 + \sum_{n=0}^{\infty}\sum_{m=0}^{n}\frac{(-1)^n}{nA^{2n}}\binom{m}{n}A^{n-m}\mathrm{Tr}\{\hat{\rho}(\hat{a}^\dagger(t)\hat{a}(t))^n\}\\
&= \ln A^2 + \sum_{n=1}^{\infty}\sum_{m=1}^{n}\frac{(-1)^n}{nA^{2n}}\binom{m}{n}A^{n-m}\\
&\quad\times\sum_{j=1}^{m}\left\{{j \atop m}\right\}\mathrm{Tr}\{\hat{\rho}\hat{a}^\dagger(t)^n\hat{a}(t)^n\},
\end{aligned}\tag{D5}$$

where $\left\{{j \atop m}\right\}$ denotes the Stirling numbers of the second kind [78].

APPENDIX E: KK SINGLE-PHOTON TOMOGRAPHY

In this section, we describe the model used in the numerical simulation for Kramers-Kronig spectral tomography of single photons (see Fig. 4). The simulations account for losses from both the EOM and the single-photon detector, as well as noise contributions from dark counts, timing jitter, and statistical fluctuations due to the finite number of measurements.

We consider the spectral tomography of single-photon states generated by heralded atomic spontaneous parametric down-conversion sources or through cavity-stimulated Raman adiabatic passage, as these sources have a larger temporal wave packet compared to the typical single-photon detector temporal resolution. This requirement cannot be met by integrated or bulk sources, which typically exhibit temporal widths on the order of picoseconds or femtoseconds. As for the detectors, we will consider reconstruction with both APDs and superconducting nanowire single-photon detectors (SNSPDs), to demonstrate the possibility of the spectral reconstruction with various detector quantum efficiencies.

1. Time sampling and time's truncation

In our numerical simulations, we model the continuous-time wavefunction of the single-photon state at each stage of the setup, $\chi(t)$, as a discrete finite series, $\tilde{\chi}(n)$, where n spans from $-N/2$ to $N/2$, with $N+1$ representing the total number of time samples.

The wavefunction in our simulations is given by

$$\tilde{\chi}(n) = N_\chi e^{-\frac{n^2 t_s^2 B^2}{2}},\tag{E1}$$

where N_χ is a normalization factor, t_s is the sampling period (set to 1 ns), and B is the bandwidth of the single photon (taken as 40 MHz).

This wavefunction extends over approximately 25 ns, a duration that should be feasible for atomic sources [81–83]. Given the chosen bandwidth and sampling period, around $n \approx 200$ samples are sufficient to capture most (99.9%) of the Gaussian's energy.

This means that, within this time window, 99.9% of the wavefunction detection probability is present.

However, to achieve better frequency resolution, we increase the total number of samples to $N \approx 5000$ by padding the numerical wavefunction with zeros before and after the main signal.

2. Model of the electro-optic modulator

The model for the EOM accounts for both linear phase modulation and losses. The EOM applies a time-dependent phase shift to the input signal $\exp(i\varphi_{\mathrm{EOM}}(t))$, where $\varphi_{\mathrm{EOM}}(t) = \pi V(t)/V_\pi$. Here, $V(t)$ is the applied voltage and V_π is the half-wave voltage of the EOM.

For our simulation, we assume an ideal EOM with infinite linear bandwidth and amplitude range. The applied voltage is defined as

$$V(t) = -\frac{V_\pi}{\pi}\sin(\omega_{\mathrm{EOM}}t),\tag{E2}$$

corresponding to a modulation index of -1, and we will set for the numerical simulation $\omega_{\mathrm{EOM}} = 80$ MHz.

We set for the EOM a 7 dB loss, which we model as an attenuation factor $\gamma_{\mathrm{EOM}}^{-1}$ on the detection probability, translating to an amplitude attenuation factor of $\gamma_{\mathrm{EOM}}^{-1/2}$. These characteristics should be achievable with current electro-optic modulators [63,65,66]. Therefore, the EOM output is a discrete signal $\tilde{\chi}_{\mathrm{EOM}}(n)$ that can be written as

$$\begin{aligned}
\tilde{\chi}_{\mathrm{EOM}}(n) &= \gamma_{\mathrm{EOM}}^{-1/2}\tilde{\chi}(n)e^{i\pi\frac{V(nt_s)}{V_\pi}} = \gamma_{\mathrm{EOM}}^{-1/2}\tilde{\chi}(n)e^{-i\sin(\omega_{\mathrm{EOM}}nt_s)}\\
&= \gamma_{\mathrm{EOM}}^{-1/2}\tilde{\chi}(n)\sum_{k=-\infty}^{\infty}J_k(-1)e^{-ik\omega_{\mathrm{EOM}}nt_s},
\end{aligned}\tag{E3}$$

where we have used $e^{iz\sin(\phi)} = \sum_n J_n(z)e^{in\phi}$ and J_k denotes the kth Bessel function of the first kind [80]. The output signal is composed of nonoverlapping aliases of the original wavefunction shifted by multiples of 80 MHz in frequency domain and weighed by the Bessel functions of first order.

3. Filtering operation

The filtering operation first removes unnecessary copies of the wavefunction generated after the EOM, retaining only the $k=0$ and $k=1$ components. The second function of the filtering process is to transform the $k=0$ contribution into a quasimonochromatic signal while attenuating the $k=1$ copy, making it significantly weaker than the quasimonochromatic component. Numerically, the first step is performed in the Fourier domain by zeroing out all frequency components outside the range $[-B/2, B/2+\omega_{\mathrm{EOM}}]$. The resulting output in the Fourier domain is given by

$$\mathcal{F}\{\tilde{\chi}_{\mathrm{filter1}}\}(\omega) = \begin{cases} 0, & \omega < -\frac{B}{2},\\ \mathcal{F}\{\tilde{\chi}_{\mathrm{EOM}}\}(\omega), & -\frac{B}{2} < \omega < \omega_{\mathrm{EOM}}+\frac{B}{2},\\ 0, & \omega > \omega_{\mathrm{EOM}}+\frac{B}{2}. \end{cases}\tag{E4}$$

The second stage of the filtering process refines the remaining $k=0$ component, reducing its bandwidth to $B_{\mathrm{mono}} = 10^6$. Simultaneously, the $k=1$ copy is attenuated by a factor of $\gamma_{\mathrm{filter}}^{-1/2} = 1/25$. The resulting output in the Fourier domain is

given by

$$\mathcal{F}\{\tilde{\chi}_{\text{filter2}}\}(\omega) = \begin{cases} 0, & \omega < -\frac{B_{\text{mono}}}{2}, \\ \mathcal{F}\{\tilde{\chi}_{\text{filter1}}\}(\omega), & -\frac{B_{\text{mono}}}{2} < \omega < \frac{B_{\text{mono}}}{2}, \\ \gamma_{\text{filter}}^{-1/2}\mathcal{F}\{\tilde{\chi}_{\text{filter1}}\}(\omega), & \frac{B_{\text{mono}}}{2} < \omega < \omega_{\text{EOM}} + \frac{B}{2}. \end{cases} \quad \text{(E5)}$$

4. Detector jitter time

The single-photon detector model in the simulation incorporates timing jitter [55]. This jitter acts as a temporal filter, $f_{\text{jitter}}(t)$, with duration t_{jitter}, applied to the time-of-arrival probability $p(t)$ that would be observed without jitter. In the continuous time domain, the jitter-affected probability is given by

$$p_{\text{jitter}}(t) = \int_{-\infty}^{\infty} \mathrm{d}\tau\, f_{\text{jitter}}(t-\tau)\, p(\tau). \quad \text{(E6)}$$

In our simulation, the jitter filter is modelled as a Gaussian with a duration $t_{\text{jitter}} = 0.1$ ns and is implemented numerically using the `gaussian_filter` function from the SciPy library. In discrete time, the jitter-affected time-of-arrival probability is expressed as

$$\tilde{p}_{\text{jitter}}(n) = (\tilde{f}_{\text{jitter}} * \tilde{p})(n), \quad \text{(E7)}$$

where $\tilde{f}_{\text{jitter}}$ is a discrete Gaussian filter truncated at four times its standard deviation, $\sigma = t_{\text{jitter}}/t_s$, and $(f * g)(n)$ denotes the discrete convolution between f and g.

5. Time-of-arrival sample generation and losses

For each emission, the density of probability of the time of arrival is measured with the single-photon detector. These times are sampled to the sampling period t_s and are put in a histogram, which approximates the time-of-arrival probability $p_{\text{jitter}}(t)$.

Numerically, we generate samples of indices n following the probability distribution $\tilde{p}_{\text{jitter}}(n)$. This is done by generating a random uniform number x between zero and one and taking the index j such that $\sum_{j=-N/2}^{n-1} p_{\text{jitter}}(j) < x$ and $\sum_{j=-N/2}^{n} p_{\text{jitter}}(j) > x$. If there is no such n_{det}, then we assume that no photon has been measured. The index n_{det} corresponds to the time interval $[n_{\text{det}}t_s, (n_{\text{det}}+1)t_s]$ at which a single photon would have been measured. To account for the losses η, we multiply the time-of-arrival probability by $\eta < 1$, increasing thus the probability that no index n_{det} satisfies the abovementioned conditions, and thus that no photon is measured. The probability of finding no n_{det} matching the conditions corresponds in the end to the total loss of the experiment. Finally, all the samples are gathered and a histogram approximating $\tilde{p}_{\text{jitter}}(n)$ is obtained.

6. Dark count model

Additionally to the time sampling of the single-photon density probability, dark counts have been taken into account using a Poissonian statistics model, as a first approximation [101–103]. For a more precise model of the dark counts, single-photon detector dead time must be taken into account as shown in Ref. [103]. For the model we use, the probability

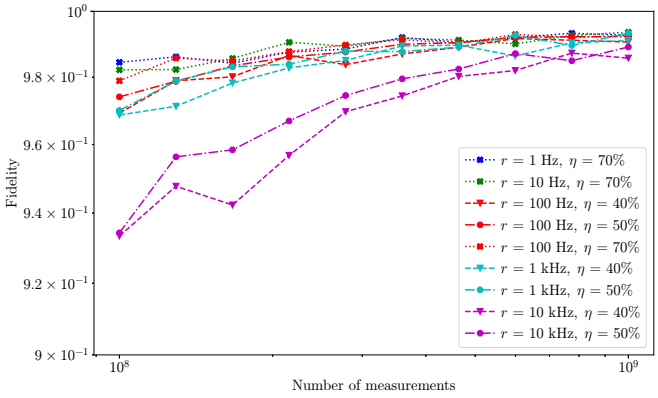


FIG. 5. Fidelity vs number of measurements taking into account all the clicks of the photodetector in the histogram reconstruction. η denotes the efficiency of the detector used in the simulation and r denotes the dark counts rate. In the simulations, the sampling rate is set to 1 GHz and the jitter of the photodetector is modelled by a Gaussian of duration 0.1 ns. For lower efficiency and higher dark count rates, more repetition of the experiments is needed to reach a target fidelity.

of having no dark count in a time slot t_s is e^{-rt_s}, where r is the dark counts rate. Therefore, the probability of dark count occurring during each time slot t_s is

$$p_{\text{dc}} = 1 - e^{-rt_s} \approx rt_s, \quad \text{(E8)}$$

where the approximation is based on the fact that the sampling rate 1 GHz is much larger than the typical dark count rate, i.e., 1 kHz for APDs. At each iteration of the simulation, each slot undergoes a Bernoulli test to generate the dark counts. For each repetition of the experiment, we generate an index n_{det} corresponding to the single-photon detection event, as well as a list of indices $(n_{\text{dc},1}, n_{\text{dc},2}, \ldots)$ corresponding to the dark counts. We add a single count to the histogram at each detected index even in the case where n_{det} and one of the $(n_{\text{dc},1}, n_{\text{dc},2}, \ldots)$ are the same. Consequently, events with multiple clicks are not discarded, even if one arises from a dark count.

7. Simulation results

The total histogram with both the photon detection events and the dark count events is normalized and undergoes KKD digital signal processing. With the phase information, the wavefunction just before the detection $\tilde{\chi}_{\text{filter2}}(k)$ is reconstructed. The reconstruction is filtered with a low-pass filter to remove the contribution of the strong monochromatic reference. Then, the reconstructed wavefunction $\tilde{\chi}_{\text{rec}}(k)$ is frequency shifted and renormalized to match the original single-photon wavefunction. The fidelity between the reconstructed wavefunction and the original is given by

$$F = \left| \int_{-\infty}^{\infty} \mathrm{d}t\, \chi(t) \chi_{\text{rec}}^*(t) \right|^2 \approx \left| \sum_{n=-N/2}^{N/2} \tilde{\chi}(n) \tilde{\chi}_{\text{rec}}^*(n) \right|^2. \quad \text{(E9)}$$

Figures 4(b) and 4(c) are examples of reconstructed wavefunction modulus and phase in the temporal domain. In this simulation, 10^8 has been taken into account. The detector has

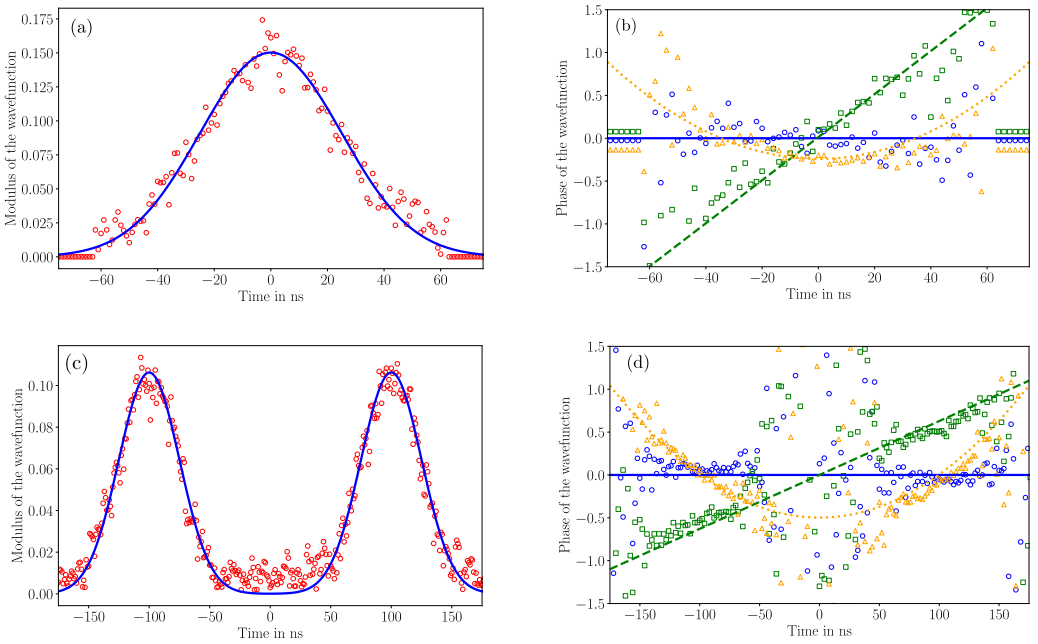


FIG. 6. Single-photon spectral tomography of (a), (b) Gaussian wavefunction and (c), (d) coherent superposition of two Gaussians with zero, linear, and quadratic phases. For each modulus plot (a)–(c), the solid (blue) curve is the original wavefunction's modulus whereas the circle (red) marks correspond to the reconstruction. For each phase reconstruction plot (b)–(d), the curves correspond to the original phases and the markers correspond to the reconstructions. The blue solid line and circle markers correspond to the case where there is no phase, the green dashed line and square markers correspond to a linear phase evolution, and finally the orange dotted line and triangle markers correspond to a quadratic phase. For each phase plot, the reconstruction matches the original as long as the associated amplitude is not small. For example, in the coherent superposition of two time-of-arrival single-photon state, the phase reconstructed seems uncorrelated to the original in between the two peaks. For every phase, we fixed the average at zero to cancel any global phase factor from the original phase of the reconstruction, which does not affect the fidelity of the reconstruction.

a jitter time of 0.1 ns, a quantum efficiency of 40%, and a dark count rate of 1 kHz, which are typical values for APDs. The fidelity of the reconstruction in this case is 96%.

In Fig. 5, we plot the fidelity of the reconstruction as a function of the number of simulated experiments, N_{exp}, in the case where all detection events are considered, even when an iteration records more than two clicks. We analyze different photodetector efficiencies η and dark count rates r, selecting values representative of commonly used detectors: APDs with $\eta \approx 40\%$ and SNSPDs with $\eta \approx 70\%$. For APDs, where $\eta = 40\%$ and r is on the order of 1 kHz, approximately 3×10^8 measurements are sufficient to reach a fidelity of 98%. In contrast, for SNSPDs with $\eta = 70\%$ and r around 1 Hz, 10^8 measurements appear to be enough to achieve the same fidelity. However, at a high number of measurements, the fidelity appears to plateau, suggesting a limiting factor beyond statistical noise. This limitation may stem from the nonzero dark count rate, which introduces additional noise in the measurements that does not diminish with increasing experiment repetitions.

8. Reconstruction of other single-photon wavefunctions

In this section, we showcase simulation results of the single-photon spectral tomography protocol for various wavefunction shape and phases. For all the wavefunctions, we simulated 5×10^8 iterations of the protocol with a 40% efficiency single-photon detector of jitter time 0.1 ns. We reach for each wavefunction a fidelity higher than 95%. In Fig. 6, we show simulation results for Gaussian wavefunctions (a and b) and coherent superposition of two Gaussian arrival times (c and d). In each case, the phase reconstruction seems valid as long as the modulus of the reference A is high enough (factor 10 at least) compared to the signal of interest. For example, in Figs. 6(c) and 6(d) the phase is well reconstructed except in between the two peaks where the corresponding modulus is smaller.

[1] C. E. Shannon, A mathematical theory of communication, Bell Syst. Tech. J. **27**, 379 (1948).

[2] W. Yan, T. Tanaka, B. Liu, M. Nishihara, L. Li, T. Takahara, Z. Tao, J. C. Rasmussen, and T. Drenski, 100 Gb/s optical IM-DD transmission with 10g-class devices enabled by 65 GSamples/s CMOS DAC core, in *2013 Optical Fiber Communication Conference and Exposition and the National Fiber Optic Engineers Conference (OFC/NFOEC)* (2013), pp. 1–3.

[3] K. Zhong, X. Zhou, J. Huo, C. Yu, C. Lu, and A. P. T. Lau, Digital signal processing for short-reach optical

communications: A review of current technologies and future trends, J. Lightwave Technol. **36**, 377 (2018).
[4] K. Kikuchi, Fundamentals of coherent optical fiber communications, J. Lightwave Technol. **34**, 157 (2016).
[5] D. Malyon, Digital fibre transmission using optical homodyne detection, Electron. Lett. **20**, 281 (1984).
[6] K. Kikuchi, Phase-diversity homodyne detection of multilevel optical modulation with digital carrier phase estimation, IEEE J. Sel. Top. Quantum Electron. **12**, 563 (2006).
[7] D.-S. Ly-Gagnon, S. Tsukamoto, K. Katoh, and K. Kikuchi, Coherent detection of optical quadrature phase-shift keying signals with carrier phase estimation, J. Lightwave Technol. **24**, 12 (2006).
[8] O. E. DeLange, Optical heterodyne detection, IEEE Spectrum **5**, 77 (1968).
[9] A. Mecozzi, C. Antonelli, and M. Shtaif, Kramers–Kronig coherent receiver, Optica **3**, 1220 (2016).
[10] A. Mecozzi, C. Antonelli, and M. Shtaif, Kramers–Kronig receivers, Adv. Opt. Photon. **11**, 480 (2019).
[11] T. Harter, C. Füllner, J. N. Kemal, S. Ummethala, J. L. Steinmann, M. Brosi, J. L. Hesler, E. Bründermann, A.-S. Müller, W. Freude, S. Randel, and C. Koos, Generalized Kramers–Kronig receiver for coherent terahertz communications, Nat. Photon. **14**, 601 (2020).
[12] I. Tavakkolnia, C. Chen, Y. Tan, and H. Haas, Terabit optical wireless-fiber communication with Kramer-Kronig receiver—Part I, IEEE Commun. Lett. **26**, 1964 (2022).
[13] X. Chen, J. Cho, S. Chandrasekhar, P. Winzer, C. Antonelli, A. Mecozzi, and M. Shtaif, Single-wavelength, single-polarization, single- photodiode Kramers-Kronig detection of 440-gb/s entropy-loaded discrete multitone modulation transmitted over 100-km SSMF, in *2017 IEEE Photonics Conference (IPC) Part II* (IEEE, Orlando, FL, 2017), pp. 1–2.
[14] X. Chen, C. Antonelli, S. Chandrasekhar, G. Raybon, A. Mecozzi, M. Shtaif, and P. Winzer, Kramers–Kronig receivers for 100-km datacenter interconnects, J. Lightwave Technol. **36**, 79 (2018).
[15] A. Lorences-Riesgo, F. P. Guiomar, A. N. Sousa, A. L. Teixeira, N. J. Muga, M. C. R. Medeiros, and P. P. Monteiro, 200 G outdoor free-space-optics link using a single-photodiode receiver, J. Lightwave Technol. **38**, 394 (2020).
[16] D. Orsuti, M. Cappelletti, M. Magarotto, M. Santagiustina, A. Galtarossa, and L. Palmieri, Edge-carrier-assisted phase retrieval receivers based on alternative projections: Performance and complexity analysis, in *49th European Conference on Optical Communications (ECOC 2023)* (Institution of Engineering and Technology, Glasgow, UK, 2023), pp. 578–581.
[17] Y. Ma, M. Xiang, X. Gan, C. Wei, W. Cheng, G. Zhou, Jilong Li, Jianping Li, S. Fu, and Y. Qin, Research progress on carrier-free phase-retrieval receivers, Photonics **11**, 54 (2024).
[18] K. Banaszek, L. Kunz, M. Jachura, and M. Jarzyna, Quantum limits in optical communications, J. Lightwave Technol. **38**, 2741 (2020).
[19] J. Shapiro, H. Yuen, and A. Mata, Optical communication with two-photon coherent states—part II: Photoemissive detection and structured receiver performance, IEEE Trans. Inf. Theory **25**, 179 (1979).
[20] H. Yuen and J. Shapiro, Optical communication with two-photon coherent states—Part III: Quantum measurements realizable with photoemissive detectors, IEEE Trans. Inf. Theory **26**, 78 (1980).
[21] H. P. Yuen and V. W. S. Chan, Noise in homodyne and heterodyne detection, Opt. Lett. **8**, 177 (1983).
[22] K. Banaszek and K. Wodkiewicz, Operational theory of homodyne detection, Phys. Rev. A **55**, 3117 (1997).
[23] N. G. Walker and J. E. Carroll, Multiport homodyne detection near the quantum noise limit, Opt. Quantum Electron. **18**, 355 (1986).
[24] S. D. Personick, B.S.T.J. Brief: An image band interpretation of optical heterodyne noise, Bell Syst. Tech. J. **50**, 213 (1971).
[25] T. Gehring, C. Lupo, A. Kordts, D. Solar Nikolic, N. Jain, T. Rydberg, T. B. Pedersen, S. Pirandola, and U. L. Andersen, Homodyne-based quantum random number generator at 2.9 Gbps secure against quantum side-information, Nat. Commun. **12**, 605 (2021).
[26] C. Bruynsteen, T. Gehring, C. Lupo, J. Bauwelinck, and X. Yin, 100 Gbps integrated quantum random number generator based on vacuum fluctuations, PRX Quantum **4**, 010330 (2023).
[27] D. T. Smithey, M. Beck, M. G. Raymer, and A. Faridani, Measurement of the wigner distribution and the density matrix of a light mode using optical homodyne tomography: Application to squeezed states and the vacuum, Phys. Rev. Lett. **70**, 1244 (1993).
[28] G. Breitenbach, T. Müller, S. F. Pereira, J.-P. Poizat, S. Schiller, and J. Mlynek, Squeezed vacuum from a monolithic optical parametric oscillator, J. Opt. Soc. Am. B **12**, 2304 (1995).
[29] A. Ourjoumtsev, R. Tualle-Brouri, J. Laurat, and P. Grangier, Generating optical Schrödinger kittens for quantum information processing, Science **312**, 83 (2006).
[30] V. Delaubert, N. Treps, M. Lassen, C. C. Harb, C. Fabre, P. K. Lam, and H. A. Bachor, TEM_{10} homodyne detection as an optimal small displacement and tilt measurements scheme, Phys. Rev. A **74**, 053823 (2006).
[31] O. Pinel, J. Fade, D. Braun, P. Jian, N. Treps, and C. Fabre, Ultimate sensitivity of precision measurements with intense gaussian quantum light: A multimodal approach, Phys. Rev. A **85**, 010101 (2012).
[32] P. Jian, O. Pinel, C. Fabre, B. Lamine, and N. Treps, Real-time displacement measurement immune from atmospheric parameters using optical frequency combs, Opt. Express **20**, 27133 (2012).
[33] L. S. Madsen, V. C. Usenko, M. Lassen, R. Filip, and U. L. Andersen, Continuous variable quantum key distribution with modulated entangled states, Nat. Commun. **3**, 1083 (2012).
[34] P. Jouguet, S. Kunz-Jacques, A. Leverrier, P. Grangier, and E. Diamanti, Experimental demonstration of long-distance continuous-variable quantum key distribution, Nat. Photon. **7**, 378 (2013).
[35] E. Samsonov, R. Goncharov, M. Fadeev, A. Zinoviev, D. Kirichenko, B. Nasedkin, A. Kiselev, and V. Egorov, Coherent detection schemes for subcarrier wave continuous variable quantum key distribution, J. Opt. Soc. Am. B **38**, 2215 (2021).
[36] R. Aymeric, Y. Jaouën, C. Ware, and R. Alléaume, Symbiotic joint operation of quantum and classical coherent communications, arXiv:2202.06942.

[37] N. Jain, H.-M. Chin, H. Mani, C. Lupo, D. S. Nikolic, A. Kordts, S. Pirandola, T. B. Pedersen, M. Kolb, B. Ömer, C. Pacher, T. Gehring, and U. L. Andersen, Practical continuous-variable quantum key distribution with composable security, Nat. Commun. **13**, 4740 (2022).

[38] Y. Pietri, M. Schiavon, V. M. Acosta, B. Gouraud, L. T. Vidarte, P. Grangier, A. Rhouni, and E. Diamanti, QOSST: A Highly-Modular Open Source Platform for Experimental Continuous-Variable Quantum Key Distribution, Quantum **8**, 1575 (2024).

[39] D. Qi, X. Wang, Z. Chen, Y. Lu, and S. Yu, High-performance intermediate-frequency balanced homodyne detector for local local oscillator continuous-variable quantum key distribution, Symmetry **15**, 1314 (2023).

[40] F. Roumestan, A. Ghazisaeidi, J. Renaudier, L. T. Vidarte, A. Leverrier, E. Diamanti, and P. Grangier, Experimental demonstration of discrete modulation formats for continuous variable quantum key distribution, J. Lightwave Technol. **42**, 5182 (2024).

[41] F. Zhang, J. Zheng, H. Kang, F. Sun, Q. He, and X. Su, Quantum noise of Kramers-Kronig receiver, arXiv:2005.09082.

[42] J. G. Proakis and M. Salehi, *Digital Communications*, 5th ed. (McGraw-Hill, Boston, MA, 2008).

[43] Z. Qu and I. B. Djordjevic, High-Speed free-space optical continuous variable-quantum key distribution based on Kramers–Kronig scheme, IEEE Photon. J. **10**, 1 (2018).

[44] K. J. Blow, R. Loudon, S. J. D. Phoenix, and T. J. Shepherd, Continuum fields in quantum optics, Phys. Rev. A **42**, 4102 (1990).

[45] C. Fabre and N. Treps, Modes and states in quantum optics, Rev. Mod. Phys. **92**, 035005 (2020).

[46] Z. Chen, X. Wang, S. Yu, Z. Li, and H. Guo, Continuous-mode quantum key distribution with digital signal processing, npj Quantum Inf. **9**, 28 (2023).

[47] L. Susskind and J. Glogower, Quantum mechanical phase and time operator, Phys. Phys. Fiz. **1**, 49 (1964).

[48] J.-M. Lévy-Leblond, Who is afraid of non-Hermitian operators? A quantum description of angle and phase, Ann. Phys. **101**, 319 (1976).

[49] S. M. Barnett and D. T. Pegg, Phase in quantum optics, J. Phys. A: Math. Gen. **19**, 3849 (1986).

[50] D. T. Pegg and S. M. Barnett, Unitary phase operator in quantum mechanics, Europhys. Lett. **6**, 483 (1988).

[51] S. Barnett and D. Pegg, On the Hermitian optical phase operator, J. Mod. Opt. **36**, 7 (1989).

[52] A. Vourdas, Phase states: An analytic approach in the unit disc, Phys. Scr. **1993**, 84 (1993).

[53] M. Tsang, J. H. Shapiro, and S. Lloyd, Quantum theory of optical temporal phase and instantaneous frequency, Phys. Rev. A **78**, 053820 (2008).

[54] D. Robert and M. Combescure, *Coherent States and Applications in Mathematical Physics*, Theoretical and Mathematical Physics (Springer International Publishing, Cham, 2021).

[55] T. Legero, T. Wilk, A. Kuhn, and G. Rempe, Characterization of single photons using two-photon interference, Advances In Atomic, Molecular, and Optical Physics, **53**, 253 (2006).

[56] N. Fabre, Spectral single photons characterization using generalized hong, ou and mandel interferometry, J. Mod. Opt. **69**, 653 (2022).

[57] A. O. C. Davis, V. Thiel, M. Karpiński, and B. J. Smith, Experimental single-photon pulse characterization by electro-optic shearing interferometry, Phys. Rev. A **98**, 023840 (2018).

[58] A. O. C. Davis, V. Thiel, M. Karpiński, and B. J. Smith, Measuring the single-photon temporal-spectral wave function, Phys. Rev. Lett. **121**, 083602 (2018).

[59] V. Thiel, A. O. C. Davis, K. Sun, P. D'Ornellas, X.-M. Jin, and B. J. Smith, Single-photon characterization by two-photon spectral interferometry, Opt. Express **28**, 19315 (2020).

[60] S. Kurzyna, M. Jastrzębski, N. Fabre, W. Wasilewski, M. Lipka, and M. Parniak, Variable electro-optic shearing interferometry for ultrafast single-photon-level pulse characterization, Opt. Express **30**, 39826 (2022).

[61] Y. Lei, W. Zhao, L. Cui, and X. Li, Phase retrieval from the hong-ou-mandel dip to characterize the phase spectrum of independent pulses at the single-photon level, arXiv:2405.09808.

[62] A. Mecozzi, A necessary and sufficient condition for minimum phase and implications for phase retrieval, arXiv:1606.04861.

[63] E. Wooten, K. Kissa, A. Yi-Yan, E. Murphy, D. Lafaw, P. Hallemeier, D. Maack, D. Attanasio, D. Fritz, G. McBrien, and D. Bossi, A review of lithium niobate modulators for fiber-optic communications systems, IEEE J. Sel. Top. Quantum Electron. **6**, 69 (2000).

[64] P. Kolchin, C. Belthangady, S. Du, G. Y. Yin, and S. E. Harris, Electro-Optic modulation of single photons, Phys. Rev. Lett. **101**, 103601, (2008).

[65] S. Koeber, R. Palmer, M. Lauermann, W. Heni, D. L. Elder, D. Korn, M. Woessner, L. Alloatti, S. Koenig, P. C. Schindler, H. Yu, W. Bogaerts, L. R. Dalton, W. Freude, J. Leuthold, and C. Koos, Femtojoule electro-optic modulation using a silicon–organic hybrid device, Light Sci. Appl. **4**, e255 (2015).

[66] S. Kamada, R. Ueda, C. Yamada, K. Tanaka, T. Yamada, and A. Otomo, Superiorly low half-wave voltage electro-optic polymer modulator for visible photonics, Opt. Express **30**, 19771 (2022).

[67] R. Kumar, E. Barrios, A. MacRae, E. Cairns, E. H. Huntington, and A. I. Lvovsky, Versatile wideband balanced detector for quantum optical homodyne tomography, Opt. Commun. **285**, 5259 (2012).

[68] A. I. Lvovsky, Squeezed light, arXiv:1401.4118.

[69] X. Jin, J. Su, Y. Zheng, C. Chen, W. Wang, and K. Peng, Balanced homodyne detection with high common mode rejection ratio based on parameter compensation of two arbitrary photodiodes, Opt. Express **23**, 23859 (2015).

[70] H. A. H. Kramers, La diffusion de la lumiere par les atomes, Atti Cong. Intern. Fisica **2**, 545 (1927).

[71] F. W. King, *Hilbert transforms*, *Encyclopedia of Mathematics and its Applications No. 124–125* (Cambridge University Press, Cambridge, 2009).

[72] N. J. Higham, *Functions of Matrices: Theory and Computation*, Other Titles in Applied Mathematics (Society for Industrial and Applied Mathematics, 2008).

[73] Z. Qu and I. B. Djordjevic, Continuous variable-quantum key distribution based on Kramers-Kronig scheme, in *2018 European Conference on Optical Communication (ECOC)* (2018), pp. 1–3.

[74] S. J. van Enk and C. A. Fuchs, Quantum state of an ideal propagating laser field, Phys. Rev. Lett. **88**, 027902 (2001).

[75] M. G. Paris, Displacement operator by beam splitter, Phys. Lett. A **217**, 78 (1996).
[76] R. J. Glauber, Photon correlations, Phys. Rev. Lett. **10**, 84 (1963).
[77] E. C. G. Sudarshan, Equivalence of semiclassical and quantum mechanical descriptions of statistical light beams, Phys. Rev. Lett. **10**, 277 (1963).
[78] T. Mansour and M. Schork, *Commutation Relations, Normal Ordering, and Stirling Numbers*, 1st ed. (Chapman and Hall/CRC, New York, 2015).
[79] J. Capmany and C. Fernández-Pousa, Quantum modeling of electro-optic modulators, Laser Photon. Rev. **5**, 750 (2011).
[80] A. Cuyt, V. Brevik Petersen, B. Verdonk, H. Waadeland, and W. B. Jones, *Handbook of Continued Fractions for Special Functions* (Springer Netherlands, Dordrecht, 2008).
[81] A. Kuhn, M. Hennrich, and G. Rempe, Deterministic single-photon source for distributed quantum networking, Phys. Rev. Lett. **89**, 067901 (2002).
[82] J. McKeever, A. Boca, A. D. Boozer, R. Miller, J. R. Buck, A. Kuzmich, and H. J. Kimble, Deterministic generation of single photons from one atom trapped in a cavity, Science **303**, 1992 (2004).
[83] P. Farrera, G. Heinze, B. Albrecht, M. Ho, M. Chávez, C. Teo, N. Sangouard, and H. de Riedmatten, Generation of single photons with highly tunable wave shape from a cold atomic ensemble, Nat. Commun. **7**, 13556 (2016).
[84] M. Ghioni, G. Armellini, P. Maccagnani, I. Rech, M. K. Emsley, and M. S. Ünlü, Resonant-cavity-enhanced single photon avalanche diodes on double silicon-on-insulator substrates, J. Mod. Opt. **56**, 309 (2009).
[85] E. Amri, G. Boso, B. Korzh, and H. Zbinden, Temporal jitter in free-running InGaAs/InP single-photon avalanche detectors, Opt. Lett. **41**, 5728 (2016).
[86] J. Wu, L. You, S. Chen, H. Li, Y. He, C. Lv, Z. Wang, and X. Xie, Improving the timing jitter of a superconducting nanowire single-photon detection system, Appl. Opt. **56**, 2195 (2017).
[87] B. Korzh *et al.*, Demonstration of sub-3 ps temporal resolution with a superconducting nanowire single-photon detector, Nat. Photon. **14**, 250 (2020).
[88] F. Marsili, V. B. Verma, J. A. Stern, S. Harrington, A. E. Lita, T. Gerrits, I. Vayshenker, B. Baek, M. D. Shaw, R. P. Mirin, and S. W. Nam, Detecting single infrared photons with 93% system efficiency, Nat. Photon. **7**, 210 (2013).
[89] J. M. Lukens and P. Lougovski, Frequency-encoded photonic qubits for scalable quantum information processing, Optica **4**, 8 (2017).
[90] J. Biele, J. F. Tasker, J. W. Silverstone, and J. C. F. Matthews, Shot-noise limited homodyne detection for MHz quantum light characterisation in the 2 μm band, Opt. Express **30**, 7716 (2022).
[91] S. Randel, D. Pilori, S. Chandrasekhar, G. Raybon, and P. Winzer, 100-Gb/s discrete-multitone transmission over 80-km SSMF using single-sideband modulation with novel interference-cancellation scheme, in *2015 European Conference on Optical Communication (ECOC)* (2015), pp. 1–3.
[92] Z. Li, M. Sezer Erkilinc, R. Maher, L. Galdino, K. Shi, B. C. Thomsen, P. Bayvel, and R. I. Killey, Two-stage linearization filter for direct-detection subcarrier modulation, IEEE Photon. Technol. Lett. **28**, 2838 (2016).
[93] H. Chen, N. K. Fontaine, J. M. Gene, R. Ryf, D. T. Neilson, and G. Raybon, Dual polarization full-field signal waveform reconstruction using intensity only measurements for coherent communications, J. Lightwave Technol. **38**, 2587 (2020).
[94] T. Pousset, M. Federico, R. Alléaume, and N. Fabre, Data for kramers-kronig detection in the quantum regime, GitHub (2025), https://github.com/ThomasPhyQ/Kramers-Kronig-detection-in-the-quantum-regime/blob/main/kk_single_photon_tomography.ipynb.
[95] R. J. Glauber and M. Lewenstein, Quantum optics of dielectric media, Phys. Rev. A **43**, 467 (1991).
[96] R. Chiao and J. Garrison, *Quantum Optics*, Oxford Graduate Texts, OUP ed. (Oxford University Press, USA, 2008).
[97] M. Wubs, L. G. Suttorp, and A. Lagendijk, Multipole interaction between atoms and their photonic environment, Phys. Rev. A **68**, 013822 (2003).
[98] M. Federico, V. Dorier, S. Guérin, and H. R. Jauslin, Space-time propagation of photon pulses in dielectric media, illustrations with beam splitters, J. Phys. B: At. Mol. Opt. Phys. **55**, 174002 (2022).
[99] P. L. García de León and J. Gazeau, Coherent state quantization and phase operator, Phys. Lett. A **361**, 301 (2007).
[100] F. S. Roux and N. Fabre, Wigner functional theory for quantum optics, arXiv:1901.07782.
[101] S. Vinogradov, T. Vinogradova, V. Shubin, D. Shushakov, and K. Sitarsky, Probability distribution and noise factor of solid state photomultiplier signals with cross-talk and afterpulsing, in *2009 IEEE Nuclear Science Symposium Conference Record (NSS/MIC)* (IEEE, Orlando, FL, 2009), pp. 1496–1500.
[102] B.-W. Tzou, J.-Y. Wu, Y.-S. Lee, and S.-D. Lin, Method to evaluate afterpulsing probability in single-photon avalanche diodes, Opt. Lett. **40**, 3774 (2015).
[103] N. Menkart, J. D. Hart, T. E. Murphy, and R. Roy, Dark current and single photon detection by 1550 nm avalanche photodiodes: Dead time corrected probability distributions and entropy rates, Opt. Express **30**, 39431 (2022).